SISTEMAS ESTELARES

Material didáctico para las clases de "*Estructura de la Vía Láctea*"

Clases teóricas dictadas por:
Dra. Lilia P. Bassino

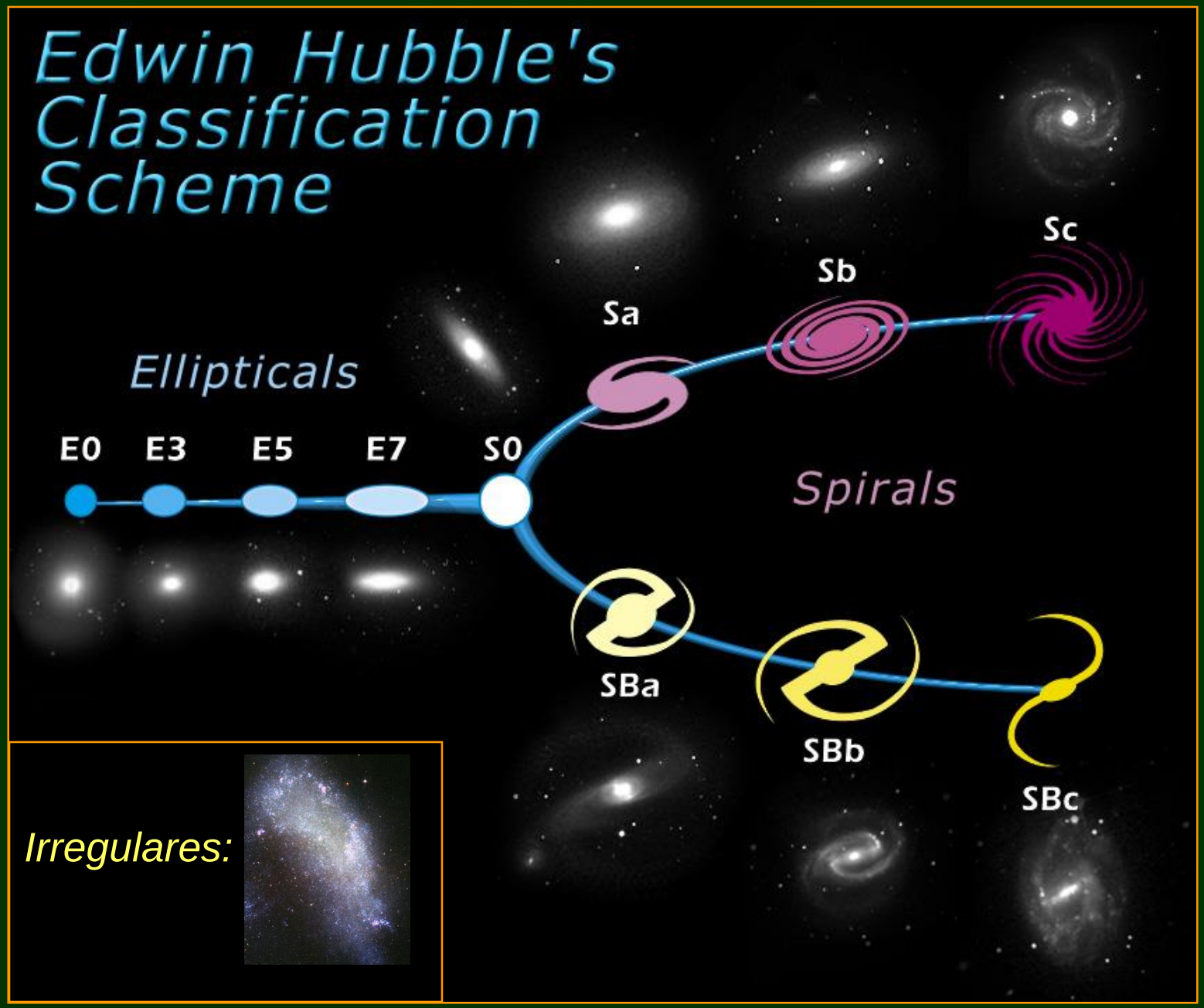
Edwin Hubble's Classification Scheme
Ellipticals
E0
E3
E5
E7
S0
Sa
Sb
Sc
Spirals
SBa
SBb
SBc
Irregulares:

Galaxia elíptica gigante M87

Cúmulo globular

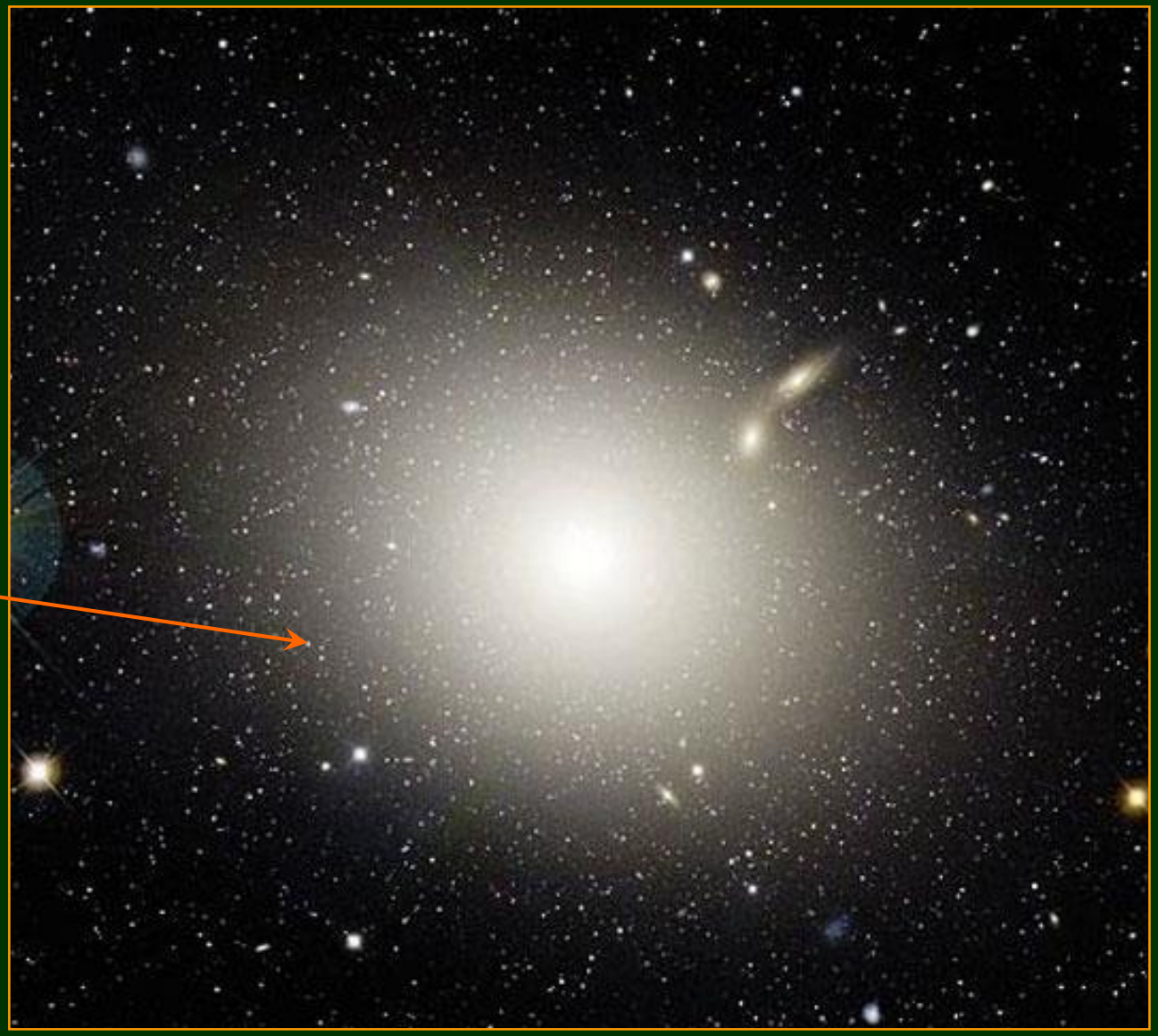

Canada-France-Hawaii Telescope, J.-C. Cuillandre (CFHT), Coelum

Distintos tipos de galaxias espirales comparadas con una galaxia irregular (arriba centro)

Courtesy Adam Block (KPNO Visitor Program), NOAO, NSF

NGC205

Galaxia espiral

Andrómeda, M31

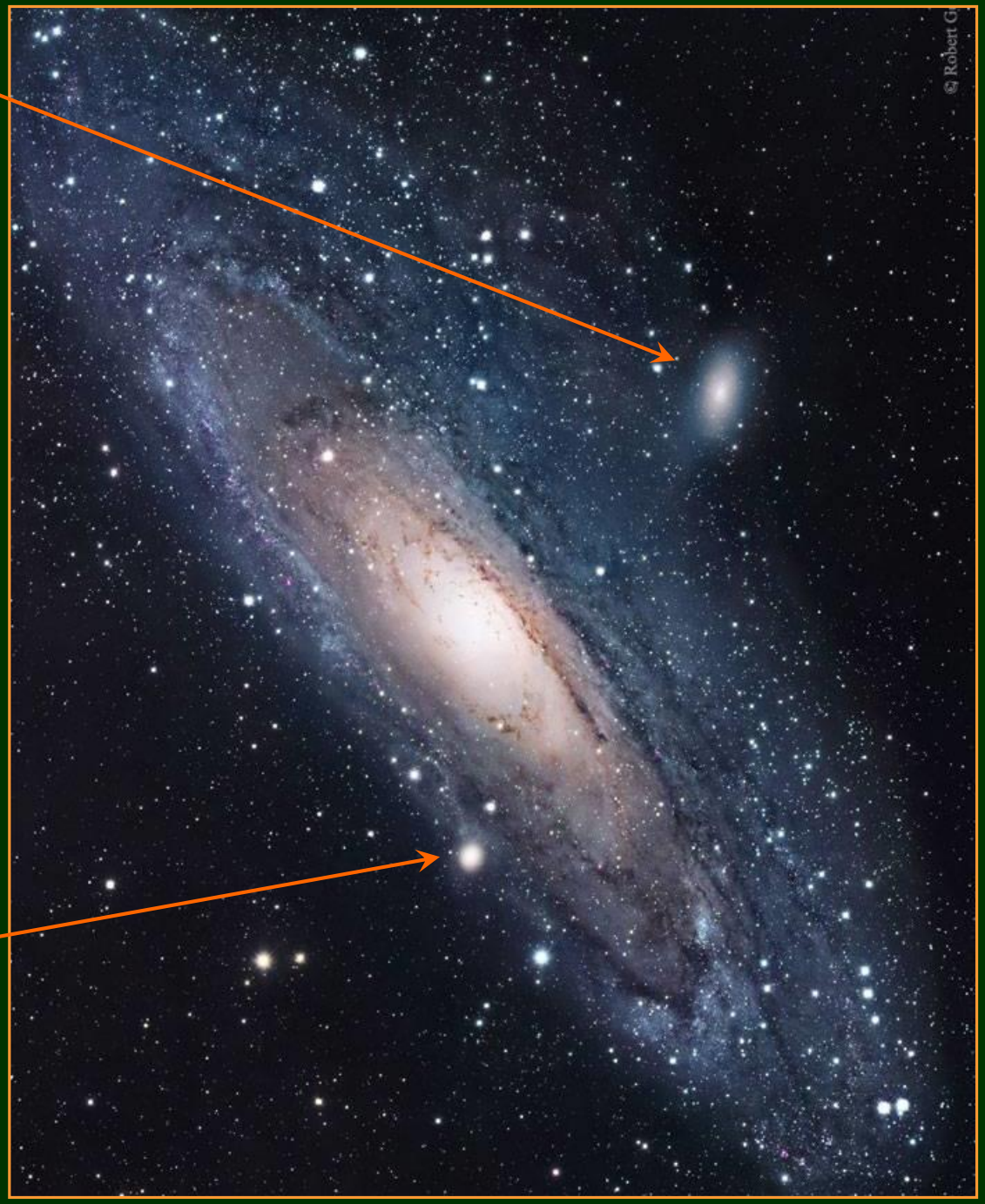

M32

Credit & Copyright: Robert Gendler
(robgendlerastropics.com)

La Vía Láctea… ¿Cómo la vemos en el cielo?

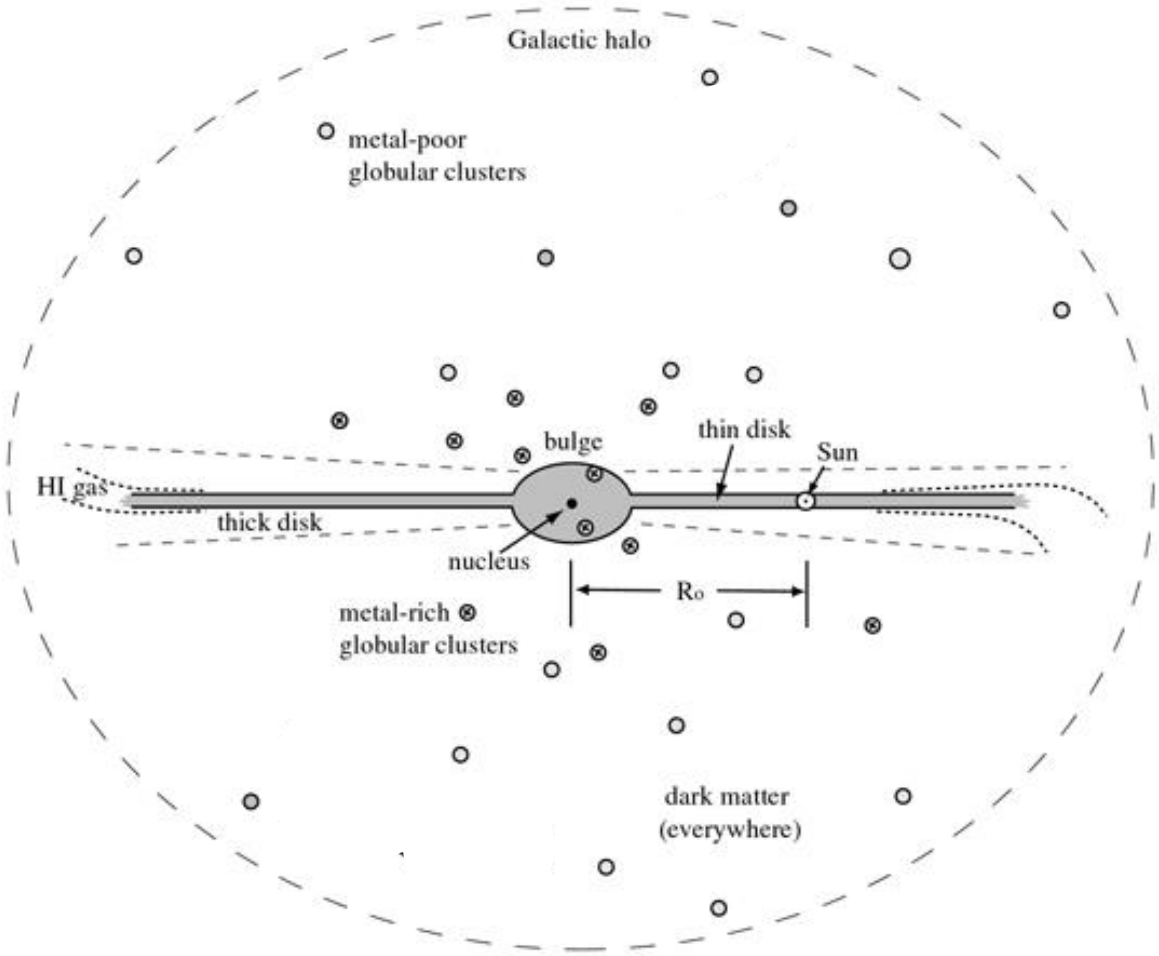

Fig 1.8 'Galaxies in the Universe' Sparke/Gallagher CUP 2007

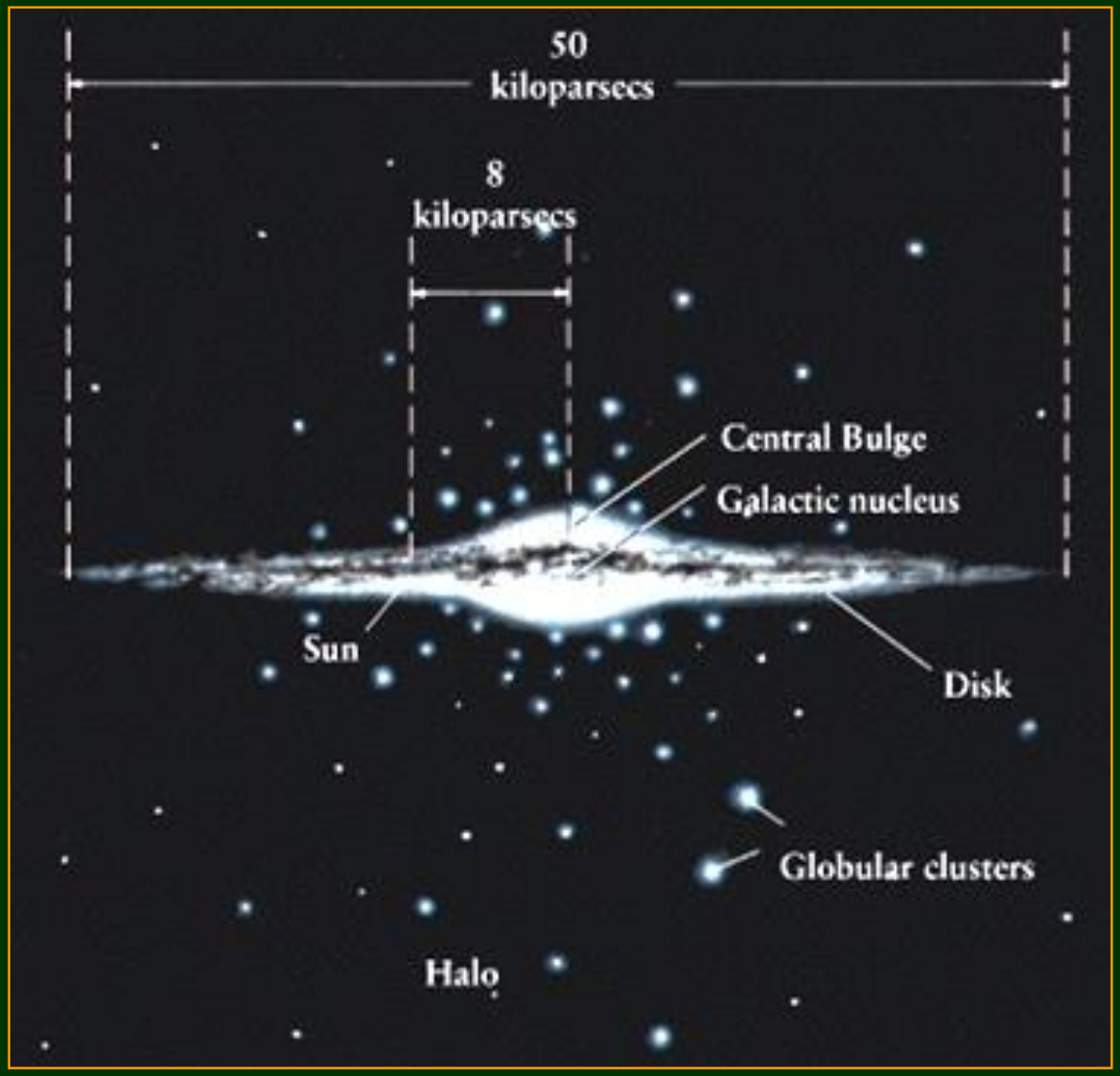
50
kiloparsecs
8
kiloparsecs
Central Bulge
Galactic nucleus
Sun
Disk
Globular clusters
Halo

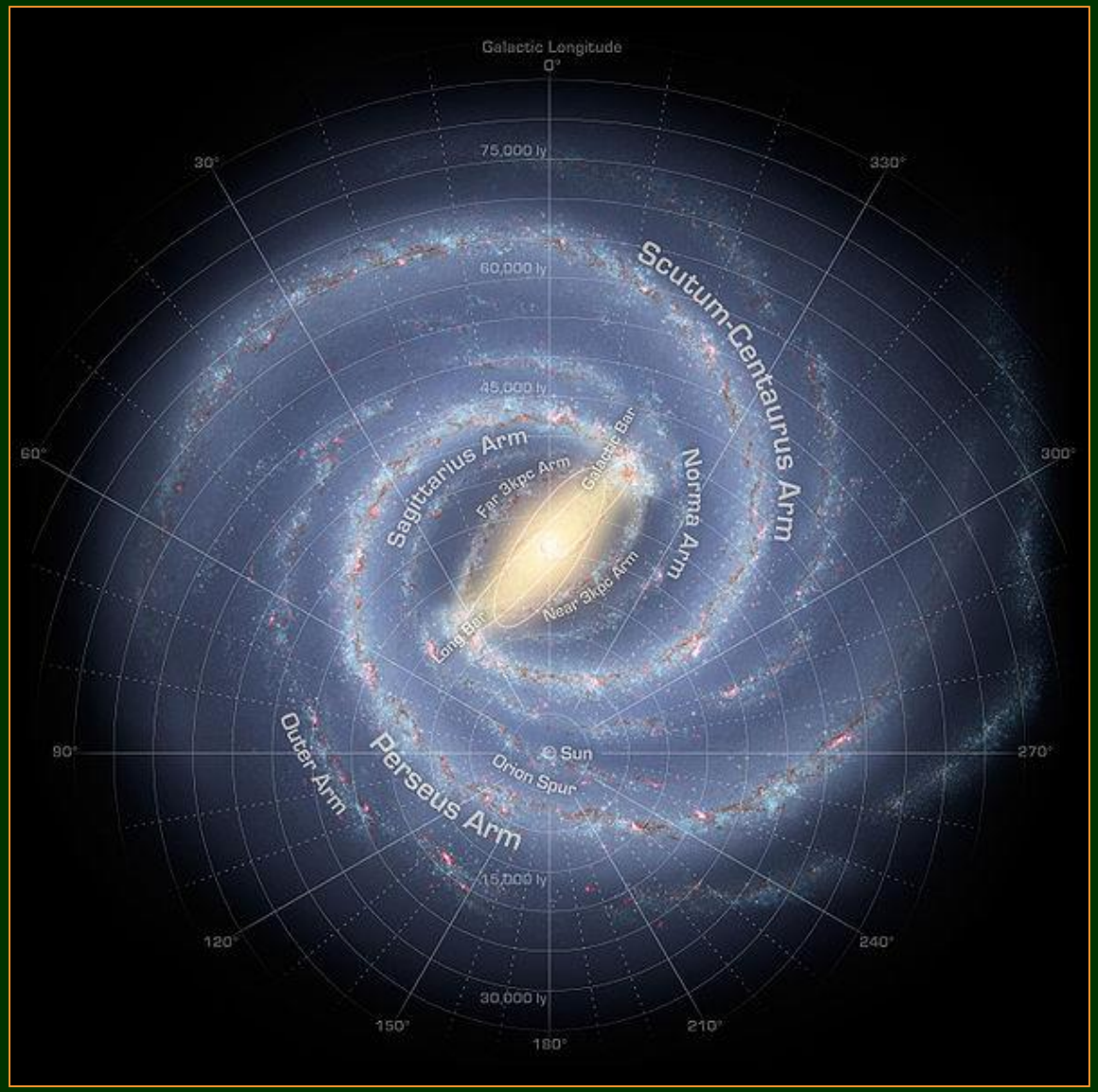

Esquema de la estructura de la Galaxia en base a datos en IR del telescopio espacìal Spitzer (NASA) **http://www.spitzer.caltech.edu/**

Galaxia espiral barrada M83

*: posición donde se ubicaría el Sol

Imagen ESO

La Vía Láctea

Se la clasifica como una **galaxia espiral barrada** (tipo SBbc)

Componente esferoidal:

- Núcleo
- Bulbo
- Halo

Componente de disco:

- Disco delgado
- Disco grueso

Barra (barra con bulbo embebido?)

Materia oscura (“halo oscuro”)

R. Kennicutt (Steward Obs.) et al.,
SSC, JPL, Caltech, NASA

The Sombrero Galaxy (VLT ANTU + FORS1)

ESO PR Photo 07a/00 (22 February 2000)

Efecto del polvo: M104 (Sa)

Imágenes: Spitzer + HST (arriba), y VLT (derecha)

Peter Barthel (Kapteyn Inst.) et al.

Bruce Hugo and Leslie Gaul,
Adam Block (KPNO Visitor Program),
NOAO, AURA, NSF

Galaxias espirales de canto

NGC 4565 (arriba) y

NGC 5746 (der., “*boxy bulge*”)

La Vía Láctea: imagen en IR cercano (del satélite COBE, NASA)

La Vía Láctea: imagen en IR cercano (del satélite COBE, NASA)

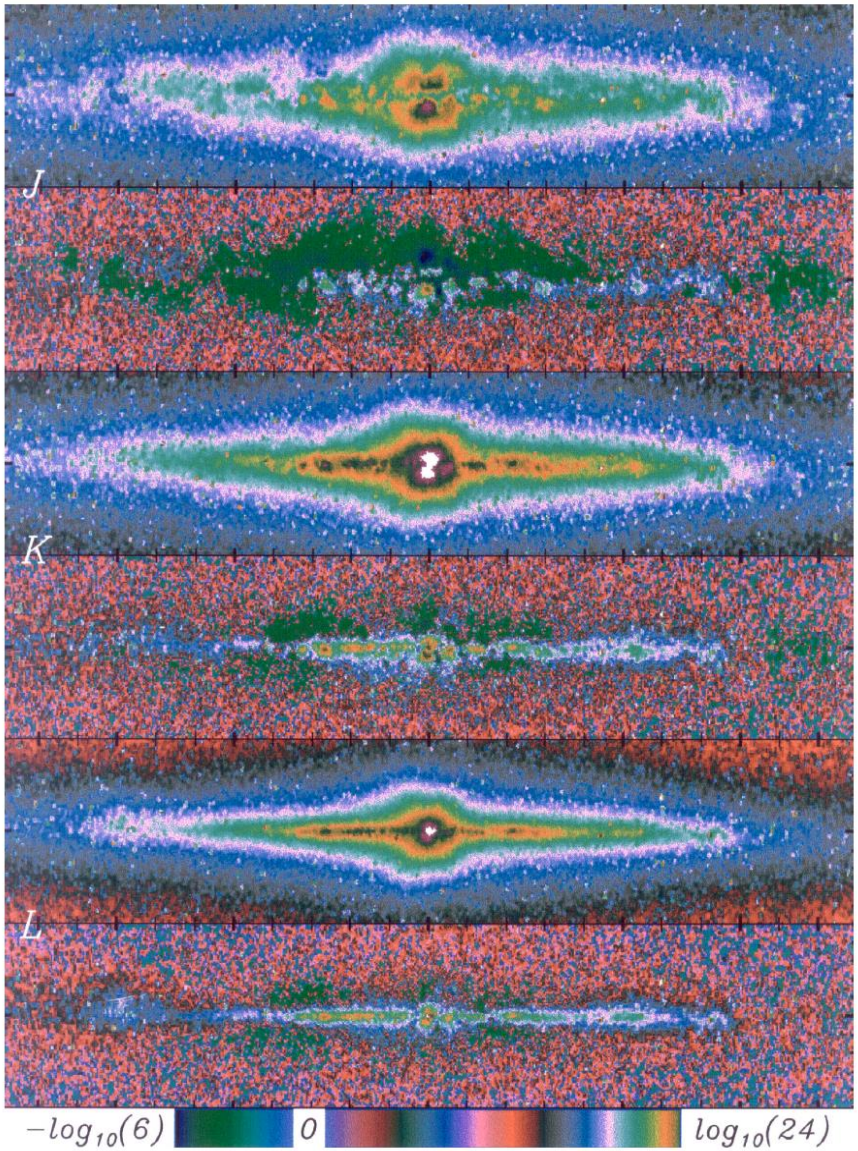

FIG. 9.—*J*-, *K*-, and *L*-band surface brightnesses [log ($|I_\nu| + 0.001$ MJy sr^{-1})] before and after the model S map was subtracted. The colors of this coded intensity image are modulated to create a contour-like effect to better show structure. Colors to the left of the break in the color bar (blue to dark green to blue) represent negative surface brightness. White pixels are saturated. The range is $l < 110°$ and $b < 15°$. Tick marks are at intervals of 10° (l) and 3° (b).

FREUDENREICH (see 492, 503)

Freudenreich 1998,
ApJ 492, 495

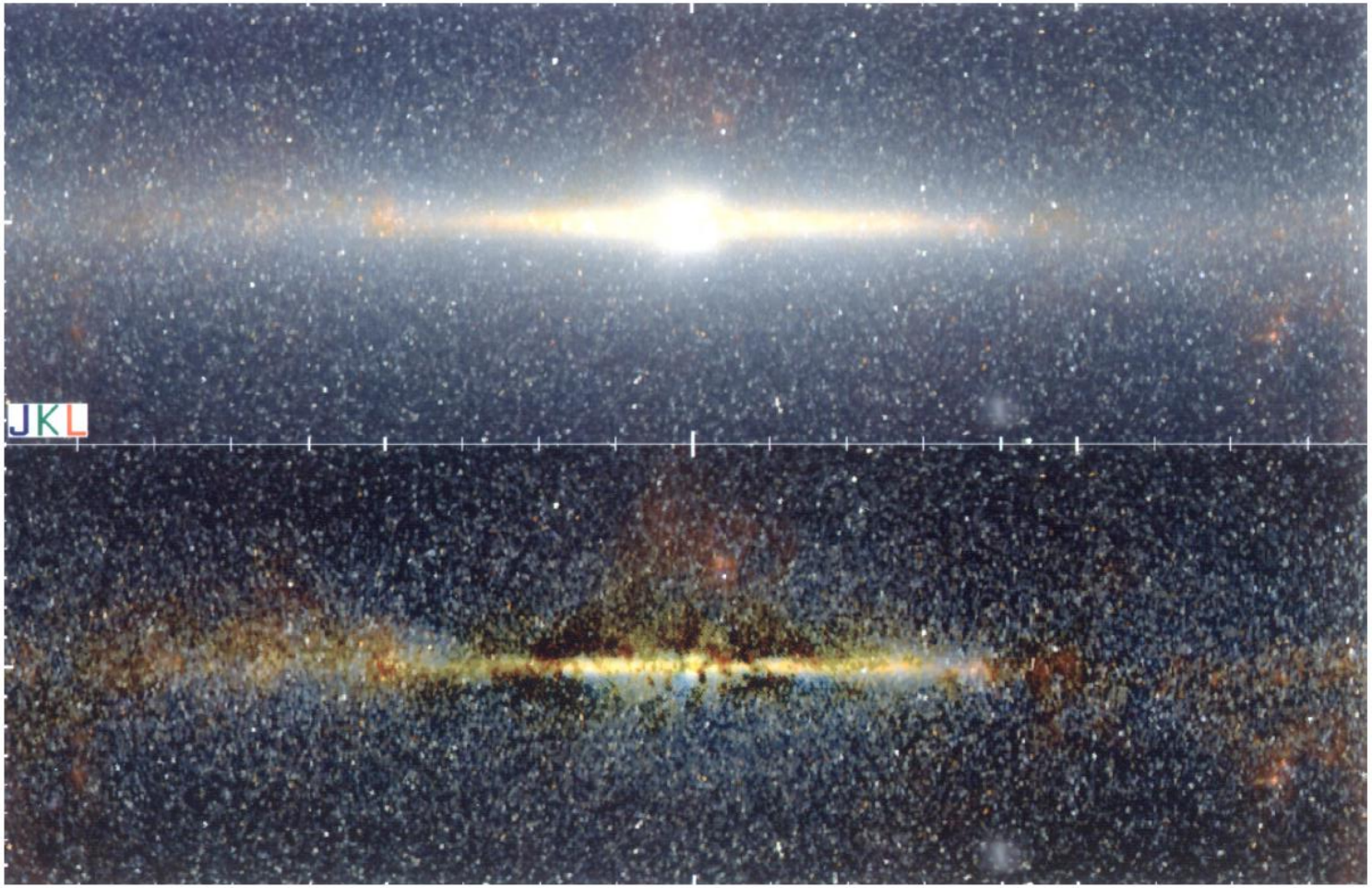

FIG. 11.—Logarithmic three-color image of the Galaxy ($|b| < 60°$) before and after model S was subtracted. The J and K bands have been scaled to the central emissivity of the L band. Tick marks are at intervals of 20° (l) and 5° (b).

FREUDENREICH (see 492, 503)

Freudenreich 1998, ApJ 492, 495

Función luminosidad de estrellas en los alrededores del Sol

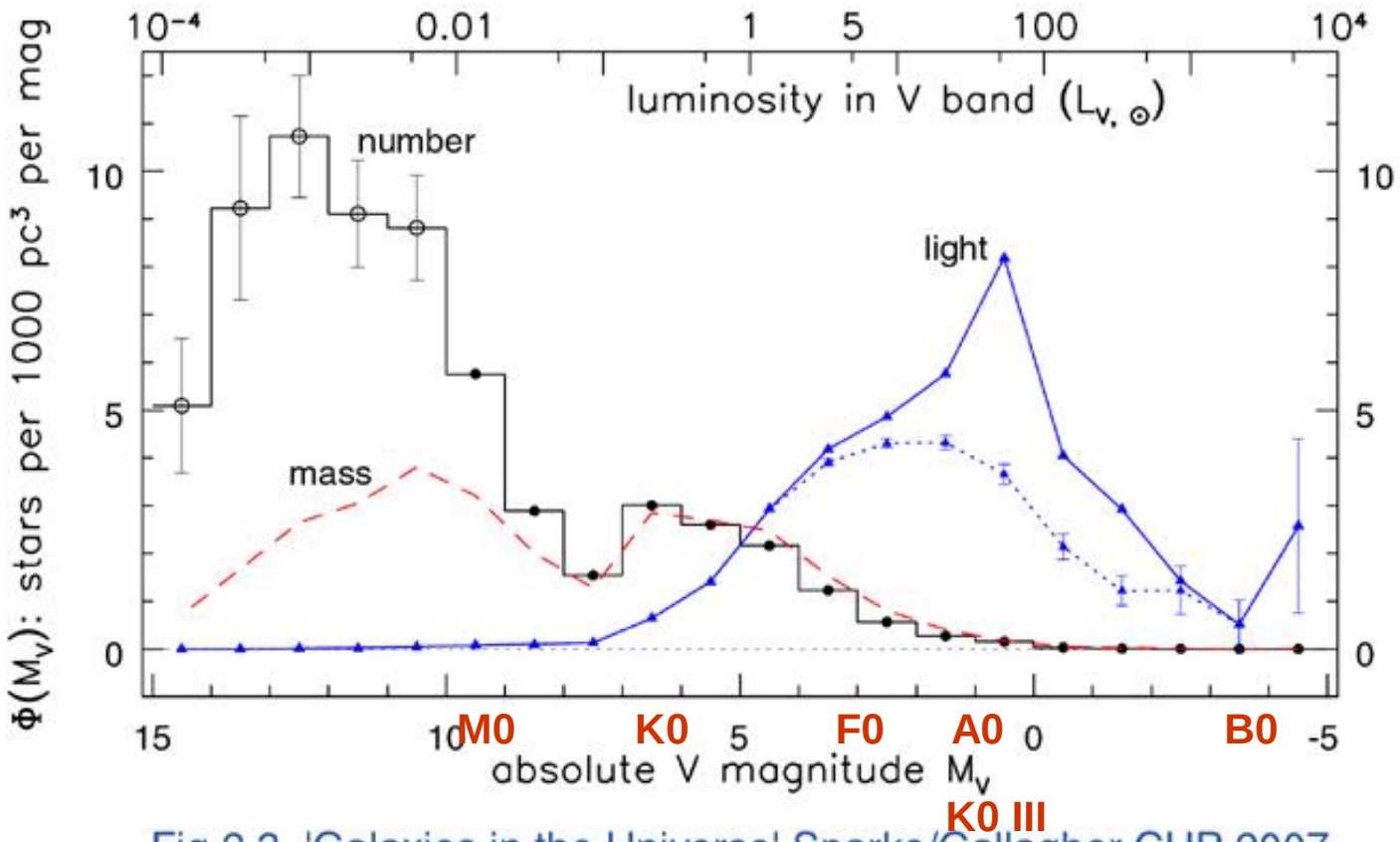

Fig 2.3 'Galaxies in the Universe' Sparke/Gallagher CUP 2007

Filtros del 2MASS (Two Micron All Sky Survey) : J, H y Ks

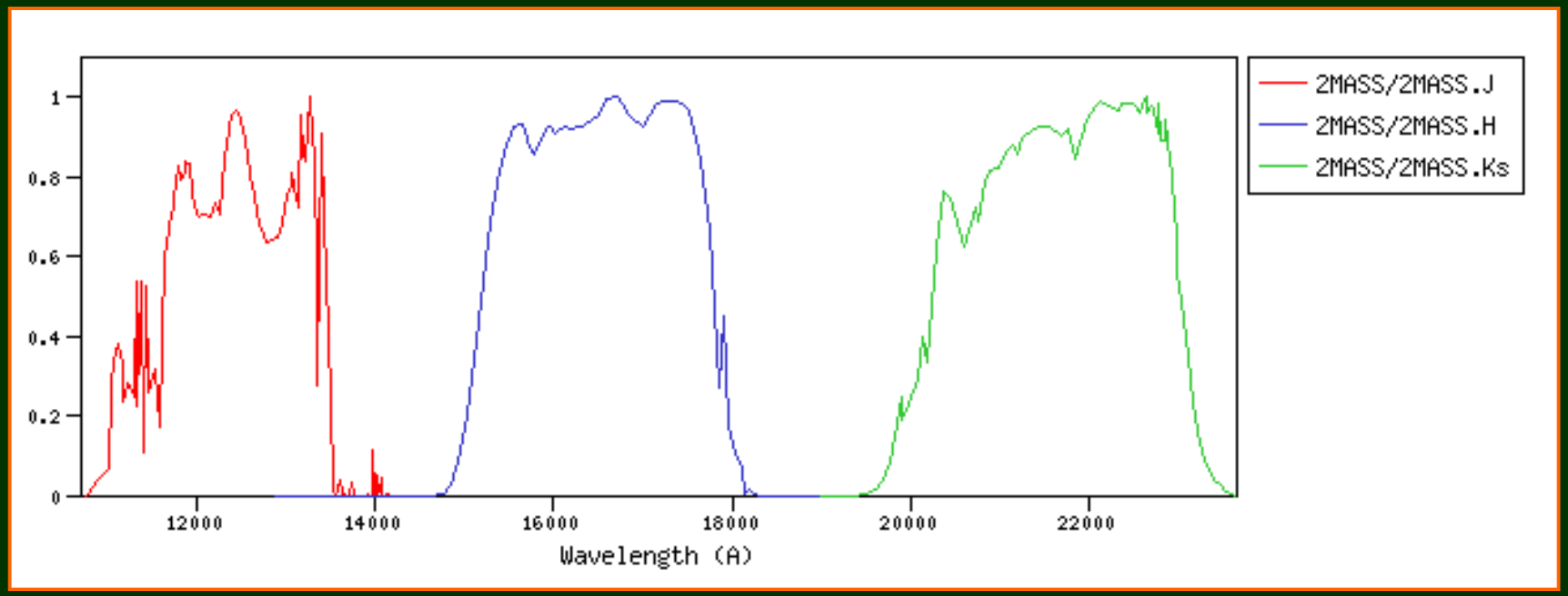

2MASS is a joint project of the University of Massachusetts and the Infrared Processing and Analysis Center/California Institute of Technology, funded by the NASA and the NSF.

Disco delgado, disco grueso y halo (conteos en función de la b)

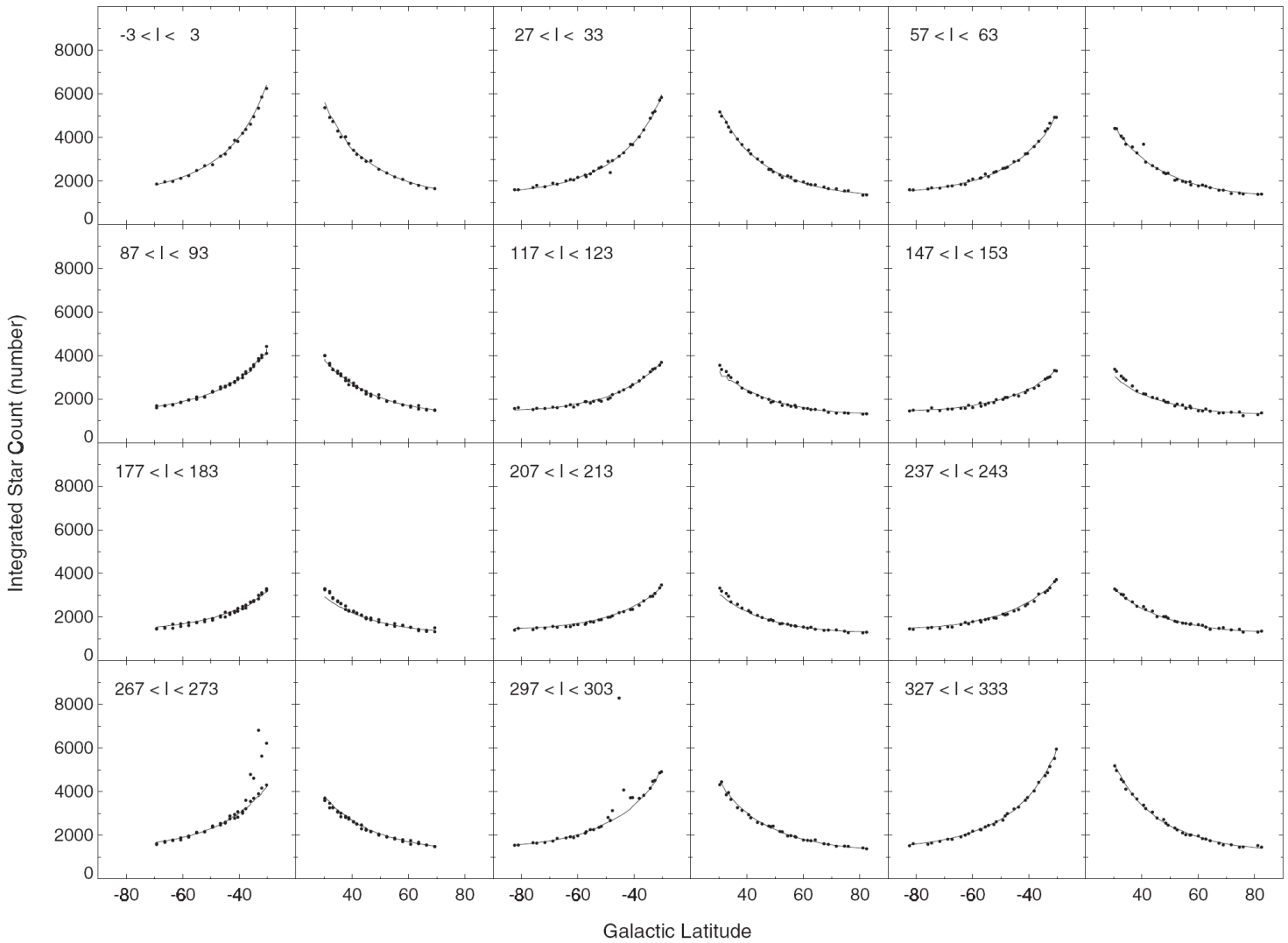

Figure 3. Integrated star count from $K_s = 5$ to 14 mag of 2MASS data as a function of the Galactic latitude. Solid line is the model prediction.

Chang et al. 2011, ApJ 740, 34 / banda Ks: 2.2 μ

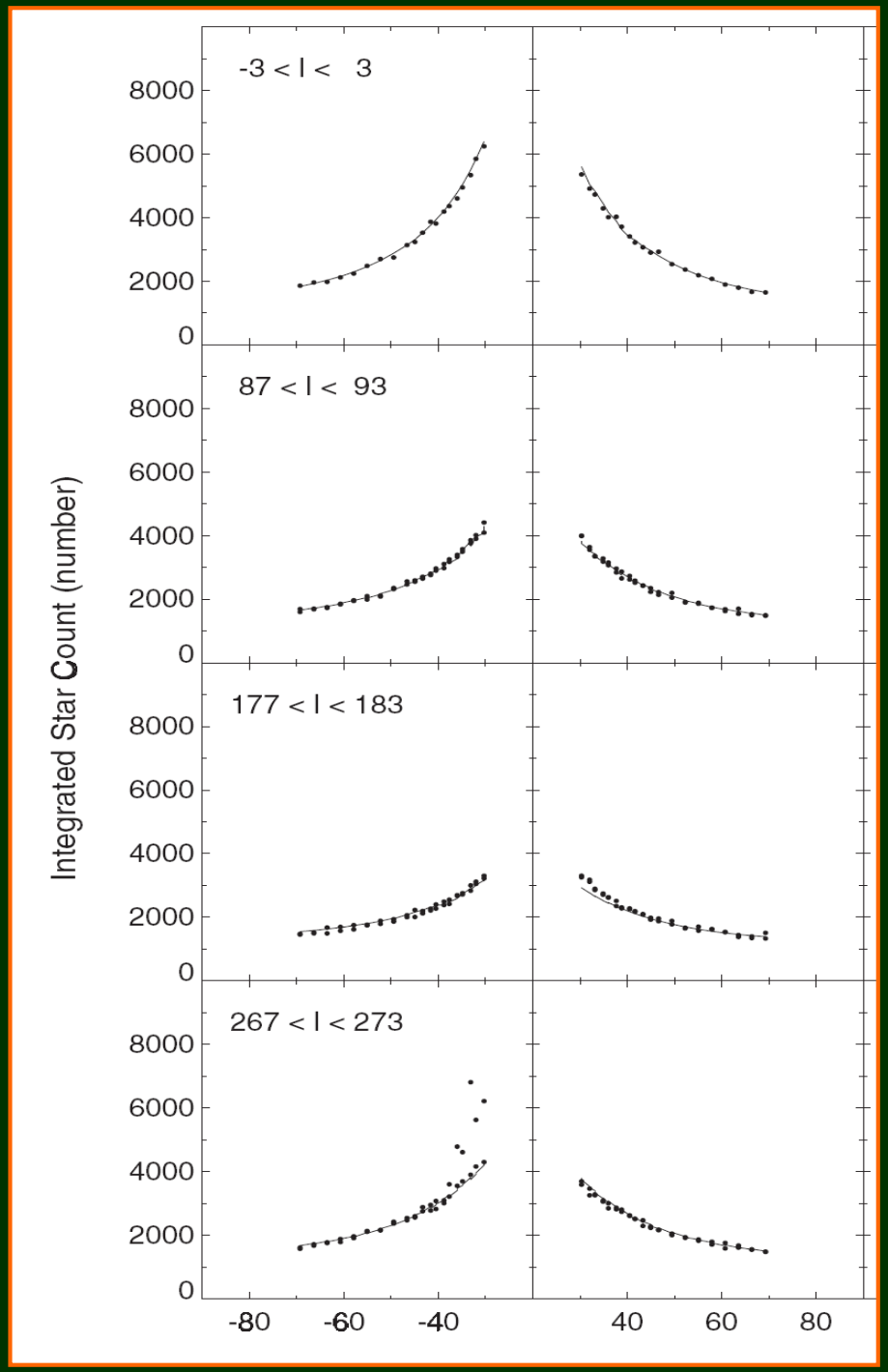

Disco delgado, disco grueso y halo (detalle de conteos en función de la b)

LMC: l ~ 280°, b ~ -33°

Chang et al. 2011, ApJ 740, 34

Disco delgado, disco grueso y halo (conteos en función de la l)

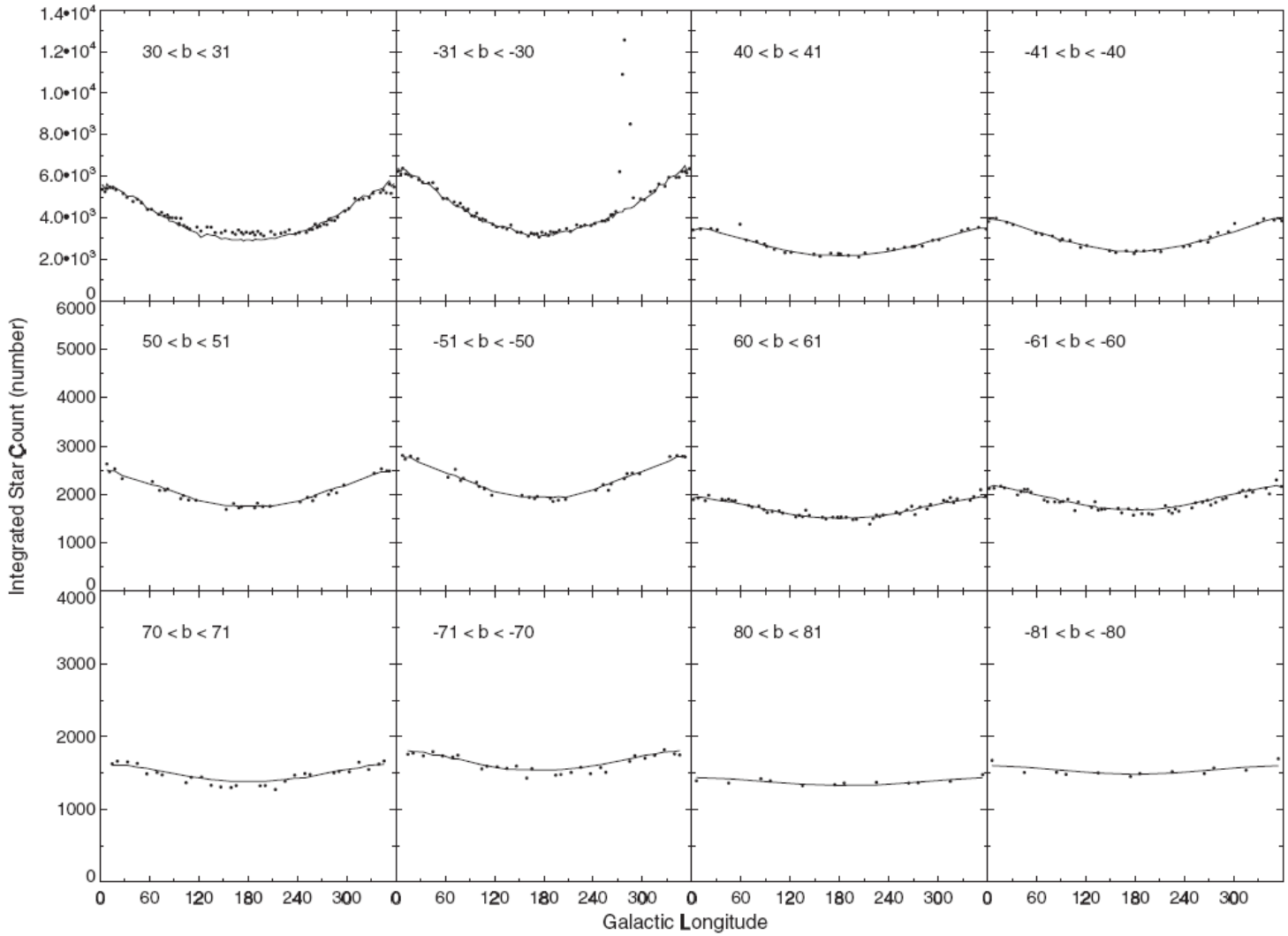

Figure 4. Integrated star count from $K_s = 5$ to 14 mag of 2MASS data as a function of the Galactic longitude. Solid line is the model prediction.

Chang et al. 2011, ApJ 740, 34

Tomografía de la Vía Láctea: distribución perpendicular al plano con conteos del SDSS

Jurić et al. 2008, ApJ 673, 864

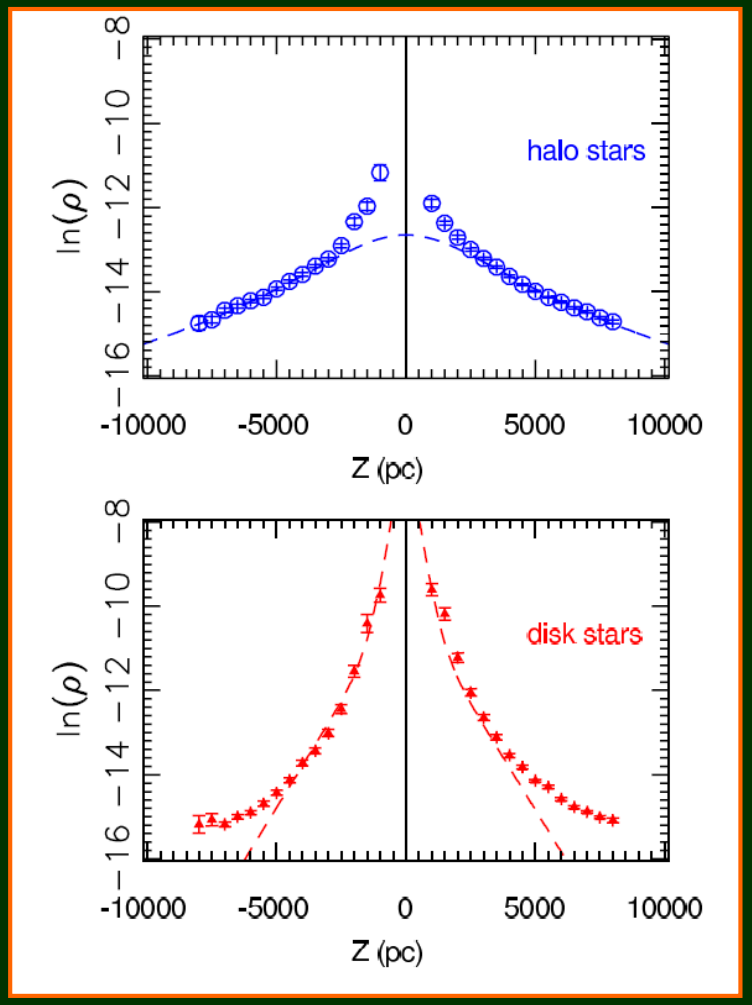

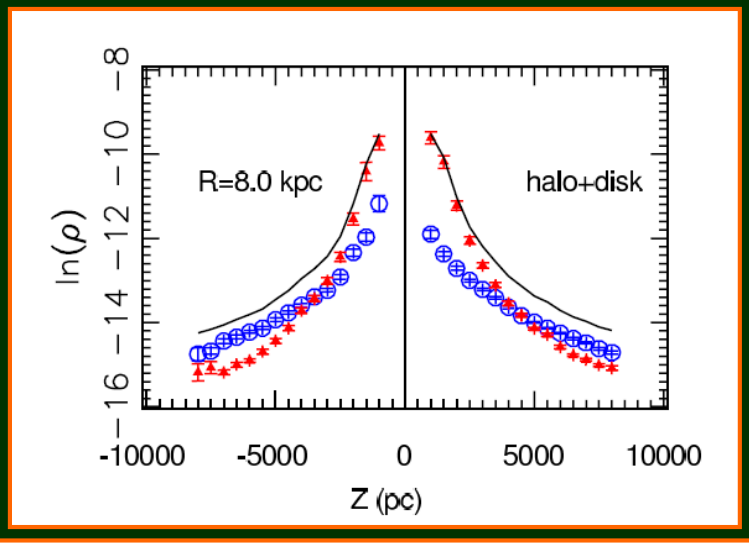

FIG. 33.— The vertical (Z) distribution of SDSS stellar counts for $R = 8$ kpc, and $0.10 < r - i < 0.15$ color bin. Stars are separated by their $u - g$ color, which is a proxy for metallicity, into a sample representative of the halo stars (low metallicity, $0.60 < u - g < 0.95$, circles) and a sample representative of the disk stars (high metallicity, $0.95 < u - g < 1.15$, triangles). The line in the top panel shows the sum of the counts for both subsamples. The counts for each subsample are shown separately in the middle and bottom panels, and compared to the best fit models, shown as lines. Note that the disk stars are more concentrated towards the Galactic plane. Due to a simple $u - g$ cut, both samples are expected to suffer from contamination: close to the Galactic plane ($|Z| < 2$ kpc) the halo sample is contaminated by the disk stars, while further away from the plane ($|Z| > 5$ kpc) the disk sample is contaminated by halo stars.

Disco delgado y disco grueso

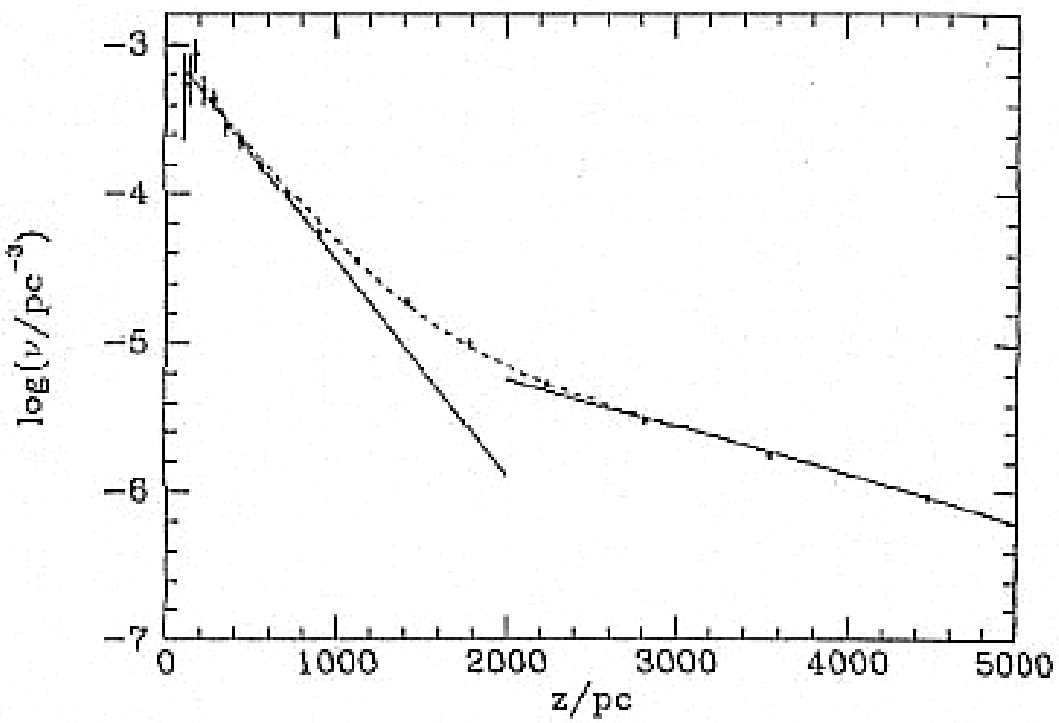

Figure 10.25 The space density as a function of distance z from the plane of MS stars with absolute magnitudes $4 \leq M_V \leq 5$. The full lines are exponentials with scale heights $z_0 = 300$ pc (at left) and $z_0 = 1350$ pc (at right). The dashed curve shows the sum of these two exponentials. [From data published in Gilmore & Reid (1983)]

Binney & Merrifield “Galactic Astronomy”

Disco delgado y disco grueso

10.4 Structure of the stellar disk

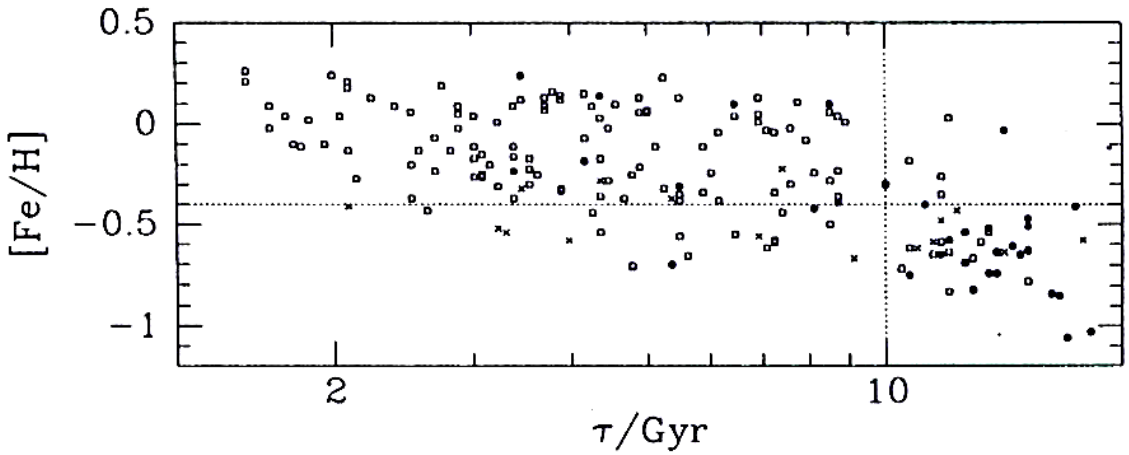

Figure 10.26 A potential division of stars between the thin and thick disks. Stars above and to the left of the dotted lines are assigned to the thin disk, while those below and to the right of the lines are assigned to the thick disk.

Binney & Merrifield "Galactic Astronomy"

Disco delgado y disco grueso: relación edad-metalicidad

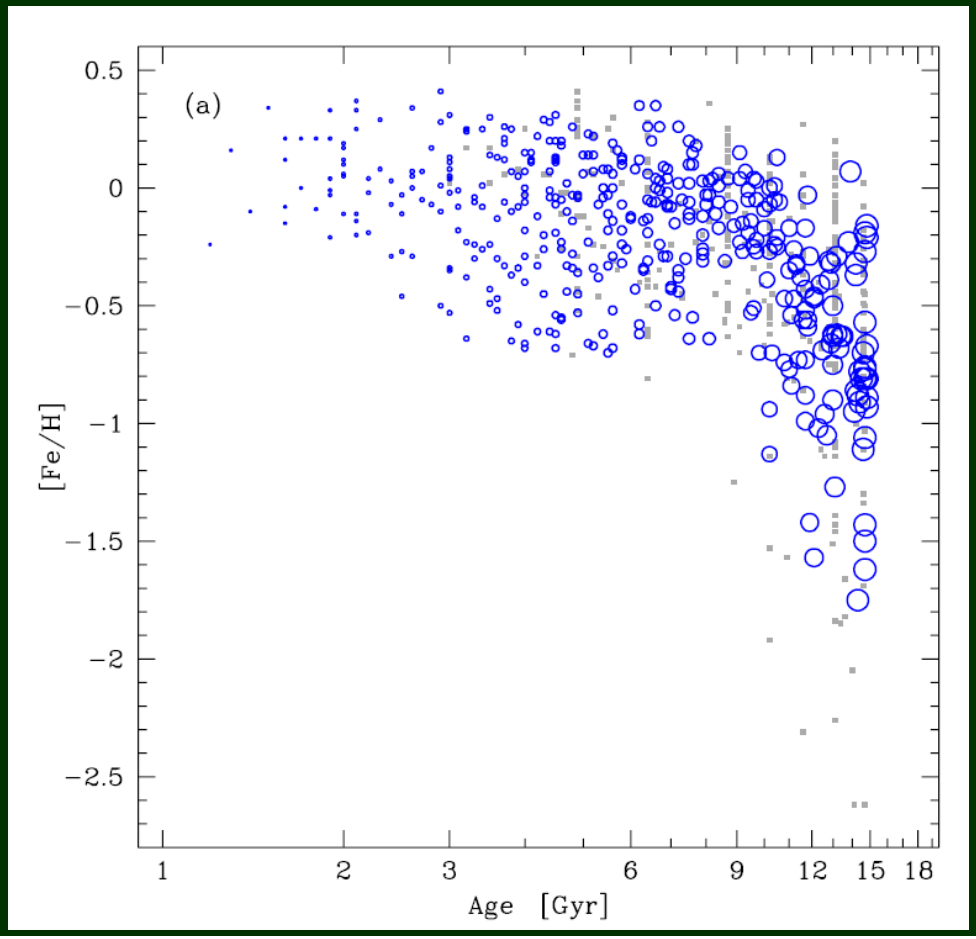

high-resolution spectroscopic study of 714 F and G dwarf and subgiant stars in the Solar neighbourhood

Fig. 21. Age-metallicity relation for those stars that have an age difference between upper and lower estimate of less than 4 Gyr. The sizes of the circles have been scaled with the ages of the stars. Stars with larger age uncertainties are shown as small grey dots.

Bensby et al. 2014, A&A 562, A71

Disco delgado y disco grueso

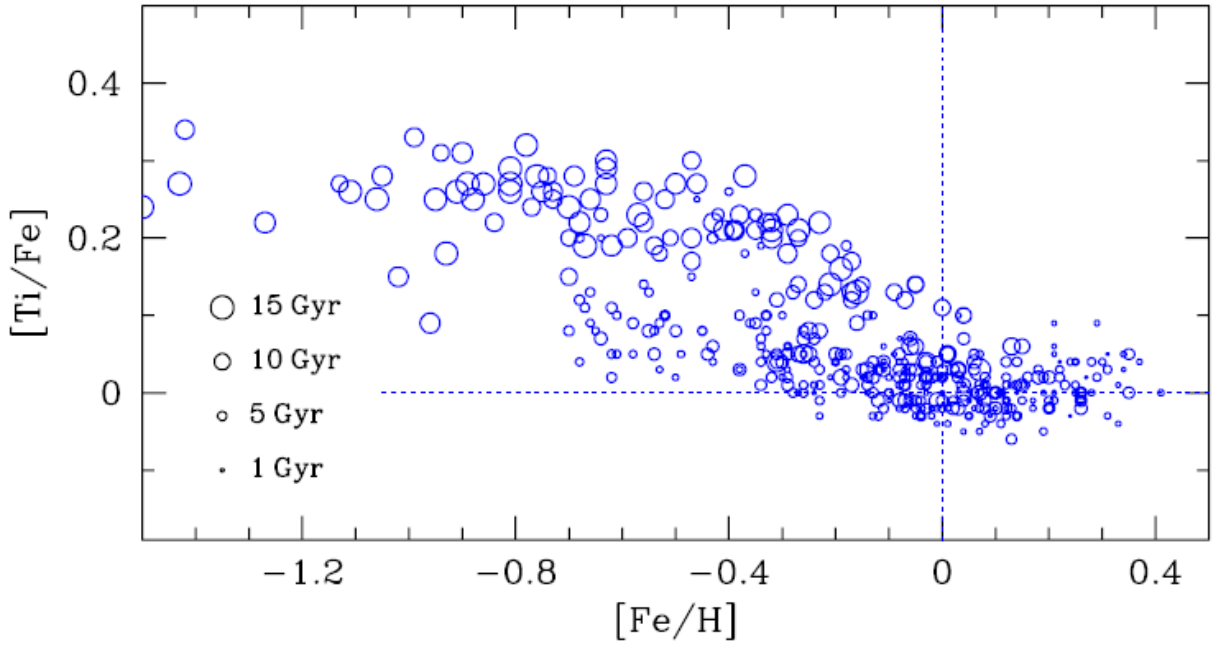

Fig. 22. [Ti/Fe] versus [Fe/H] for stars that have low age uncertainties (the differences between upper and lower age estimates are less than 4 Gyr). The sizes of the circles are scaled with the ages of the stars as indicated in the figure.

Bensby et al. 2014, A&A 562, A71

Tomografía de la Vía Láctea: densidades numéricas estelares con datos SDSS

(r - i) $\rightarrow$ F9 a M3 V

Distance:100 pc to 20 kpc, |b| > 25.

The data show strong evidence for a Galaxy consisting of an oblate halo, a disk component, and a number of localized over-densities. The number density distribution of stars as traced by M dwarfs in the Solar neighborhood (D < 2 kpc) is well fit by two exponential disks (the thin and thick disk) with scale heights and lengths:
H1 = 300 pc and L1 = 2600 pc,
H2 = 900 pc and L2 = 3600 pc

Halo: oblate models, best-fit c/a = 0.64

Jurić et al. 2008,
ApJ 673, 864

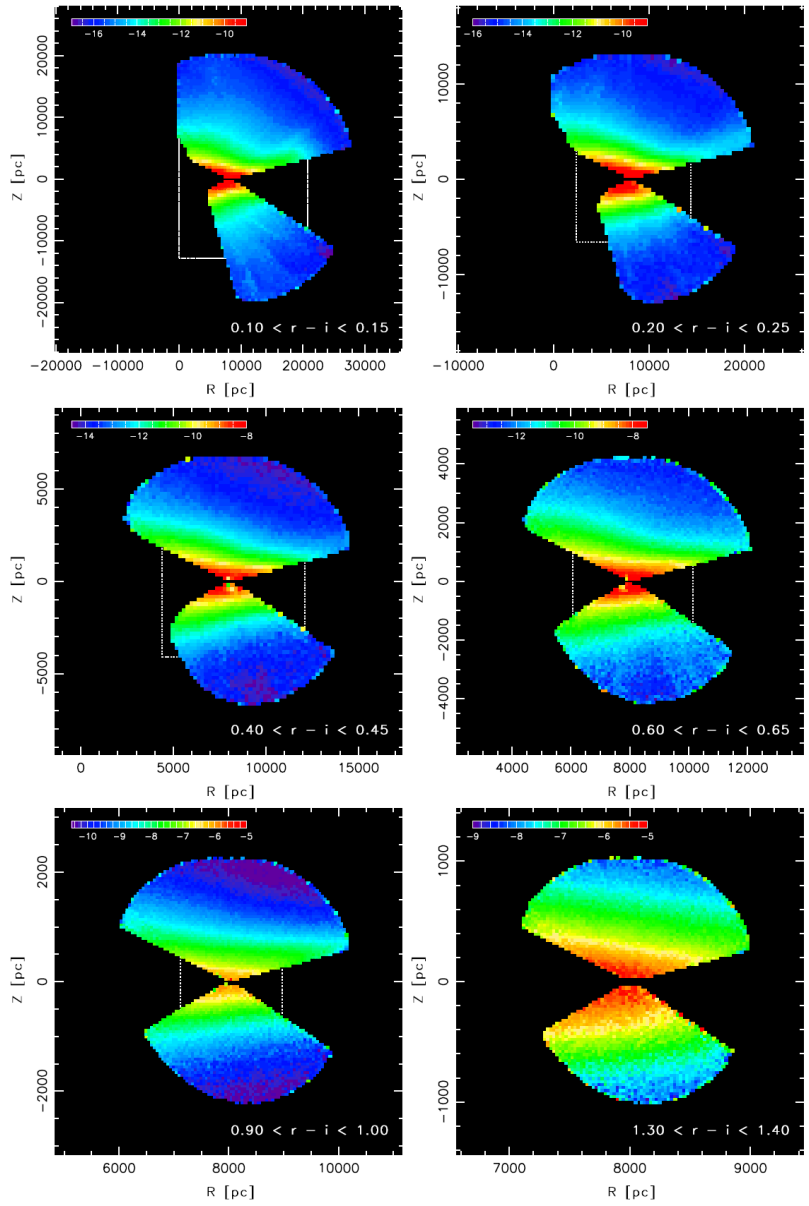

FIG. 10.— The stellar number density as a function of Galactic cylindrical coordinates R (distance from the axis of symmetry) and Z (distance from the plane of the Sun), for different $r - i$ color bins, as marked in each panel. Each pixel value is the mean for all polar angles ϕ. The density is shown on a natural log scale, and coded from blue to red (black pixels are regions without the data). Note that the distance scale greatly varies from the top left to the bottom right panel – the size of the the bottom right panel is roughly equal to the size of four pixels in the top left panel. Each white dotted rectangle denotes the bounding box of region containing the data on the subsequent panel.

Tomografía de la Vía Láctea: metalicidades estelares con datos del SDSS

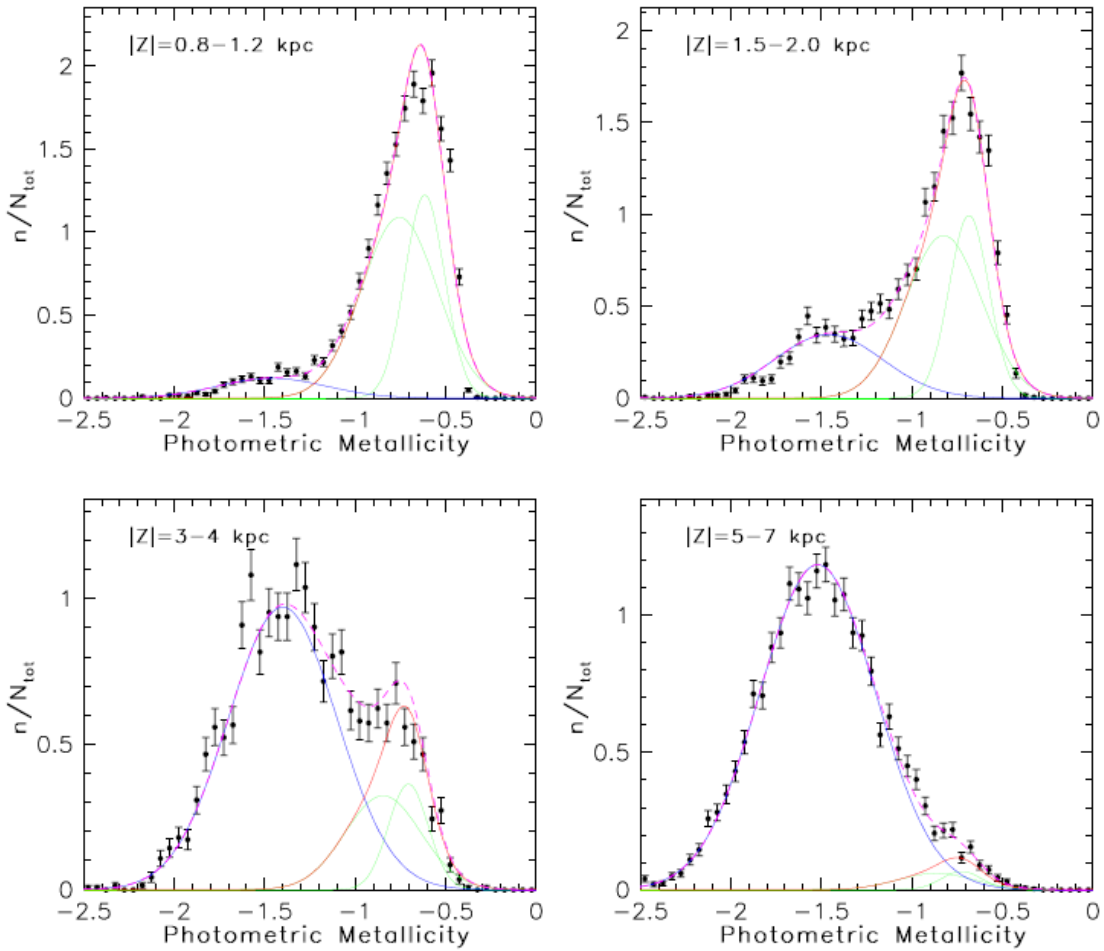

FIG. 7.— The symbols with error bars show the measured photometric metallicity distribution for stars with $0.2 < g - r < 0.4$, 7 kpc $< R <$ 9 kpc, and distance from the Galactic plane in the range 0.8–1.2 kpc (top left, ~6,200 stars), 1.5–2.0 kpc (top right, ~3,800 stars), 3.0–4.0 kpc (bottom left, ~2,800 stars) and 5.0–7.0 kpc (bottom right, ~6,000 stars). The histograms are essentially horizontal (parallel to x axis) slices at corresponding $|Z|$ intervals through the map shown in the top right panel of Figure 5. The dashed magenta lines show a best-fit two-component, halo plus disk, model. The blue lines show the halo contribution, modeled as a single Gaussian, and the red lines show the contribution of a non-Gaussian disk model, modeled as a sum of two Gaussians shown by the green lines. See § 3.3.1 and Table 3 for the best-fit parameters.

Ivezić et al. 2008, ApJ 684, 287

Tomografía de la Vía Láctea: metalicidades estelares con datos del SDSS

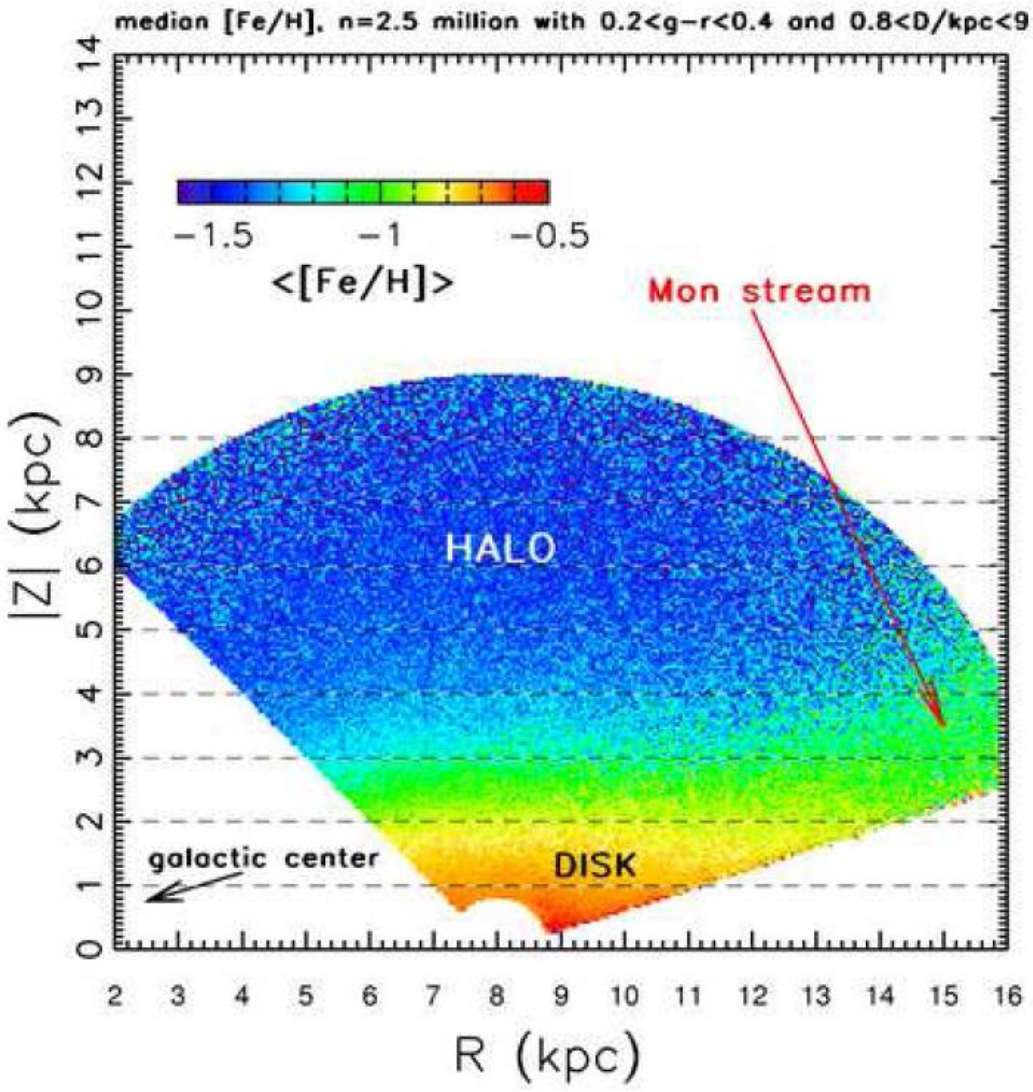

FIG. 8.— The dependence of the median photometric metallicity for ~2.5 million stars from SDSS Data Release 6 with $14.5 < r < 20$, $0.2 < g - r < 0.4$, and photometric distance in the 0.8–9 kpc range, in cylindrical Galactic coordinates R and $|Z|$ (compare to the top left panel of Figure 5). There are ~40,000 pixels (50 pc × 50 pc) contained in this map, with a minimum of 5 stars per pixel and a median of 33 stars. Note that the gradient of the median metallicity is essentially parallel to the $|Z|$ axis, except in the Monoceros stream region, as marked.

Ivezić et al. 2008, ApJ 684, 287

Valores de escala para densidad estelar recomendados por Bland-Hawthorn & Gerhard (2016)

Disco delgado

R_t: 2.6 ± 0.5 kpc, thin disk exponential radial scalelength

z_t: 300 ± 50 pc, thin disk exponential vertical scalelength at R_0

Disco grueso

R_T: 2.0 ± 0.2 kpc, thick disk exponential radial scalelength

z_T: 900 ± 180 pc, thick disk exponential vertical scalelength at R_0

Posición del Sol

z_0 = 25 ± 5 pc, distance of Sun from the Galactic Plane (Jurić et al. 2008)

Bland-Hawthorn & Gerhard 2016, ARAA 54, 529

Dos subcomponentes en el halo:

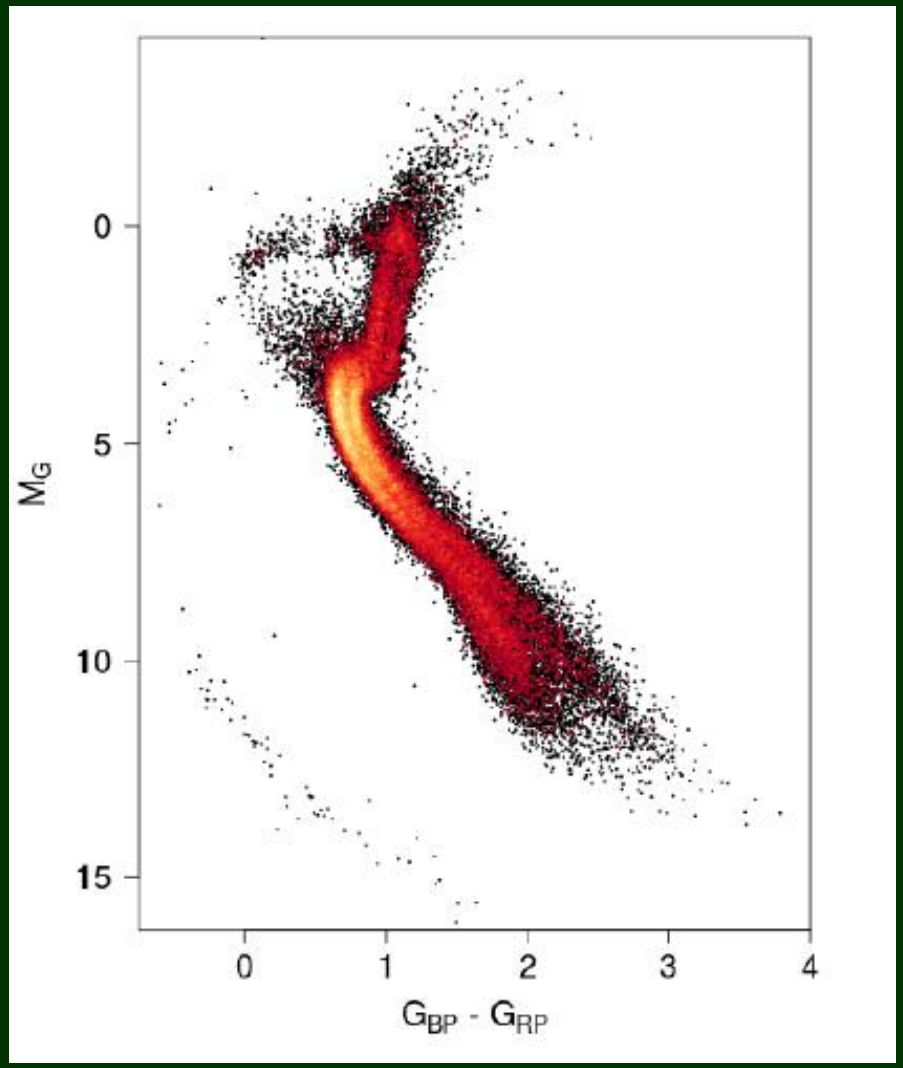

"Two different populations in a classical kinematic selection of *the halo* are unambiguously identified in the HRD"

GAIA Collab. 2018, A&A 616, A10

Valores de escala para densidad estelar recomendados por
Bland-Hawthorn & Gerhard (2016)

Halo → evidence for a *dual halo* (oblate double power-law models)

- the *inner halo* is flattened and slowly rotating,

α_{in}: -2.5 ± 0:3, inner density slope

q_{in}: 0:65 ± 0:05, inner halo flattening (c/a)

- the *outer halo* is near-spherical and retrograde rotation,

α_{out}: -4.0, outer density slope

q_{out}: 0:8 ± 0:1, outer halo flattening (c/a)

- r_s: 25 ± 10 kpc, break radius

Bland-Hawthorn & Gerhard 2016, ARAA 54, 529

Estructura espiral de M51 a partir de cúmulos estelares

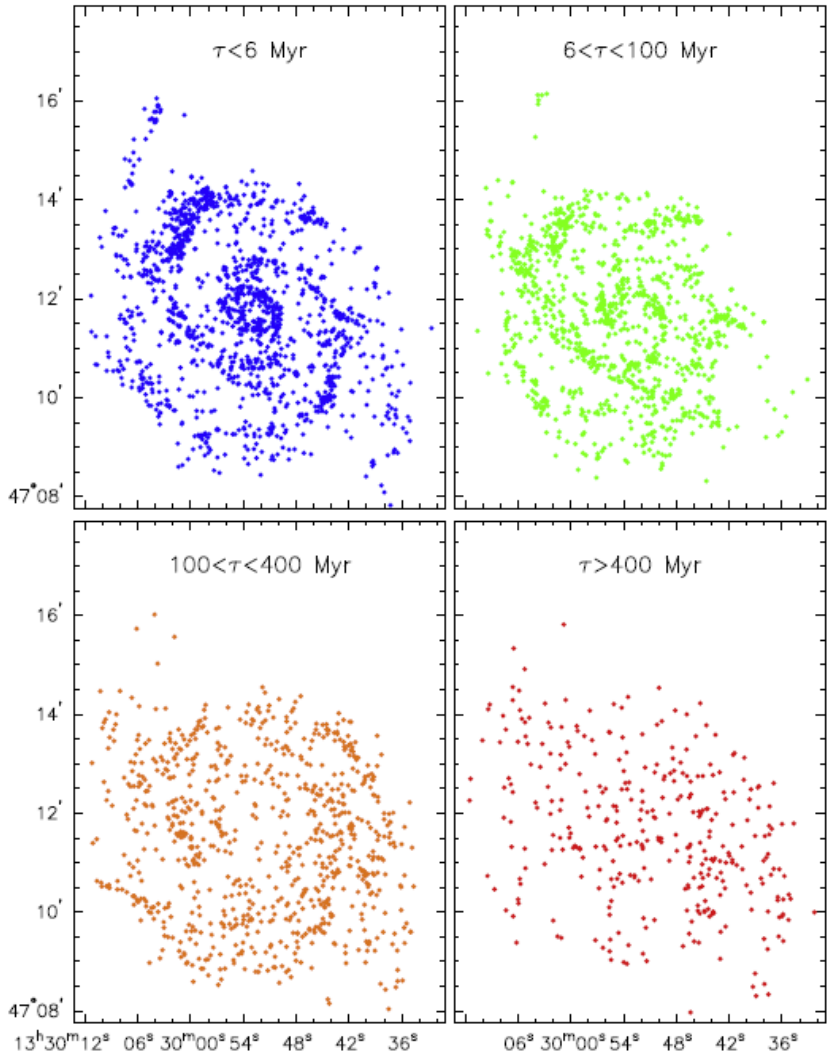

Figure 2. Gradual diffusion of clusters throughout the disk of M51. The clusters start out quite concentrated in the arms, and they become more and more dispersed as they age. Clusters with ages of a few hundred Myr do, however, still show weakly concentrated structure and are not yet fully dispersed. The color-coding is the same as in Figure 1: (<6 Myr (blue) 6–100 Myr (green); 100–400 Myr (orange); and >400 Myr (red).

imágenes multi-banda del HST

Chandar et al. 2017, ApJ 845, 78

Estructura espiral a partir de la distribución del polvo (COBE)

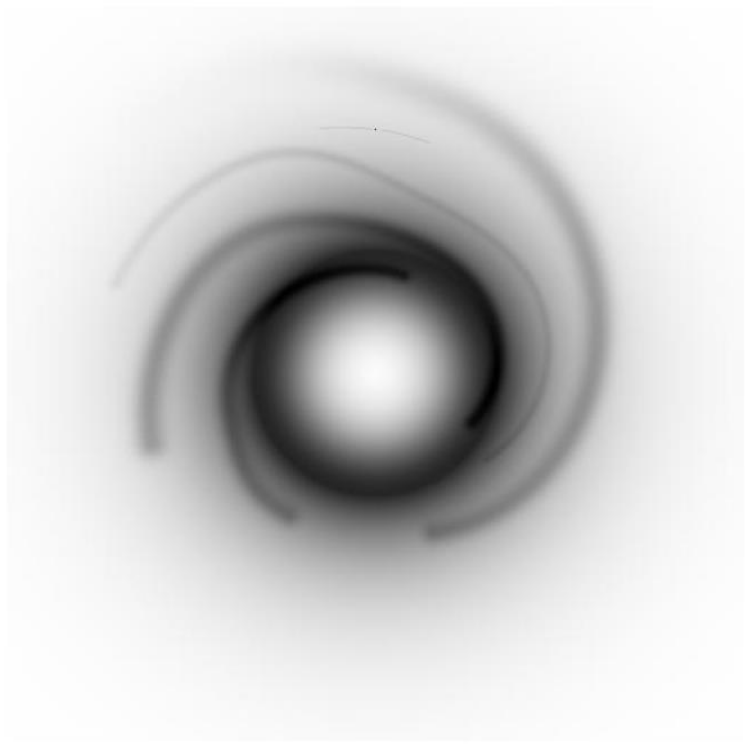

FIG. 13.—Surface density map of the dust, as inferred from the dust density model. Small black dot (*upper center*) shows the position of the Sun, which nearly lies on a small local feature, known as the Orion arm. Arms are incomplete on the side opposite the Sun owing to incomplete H II data.

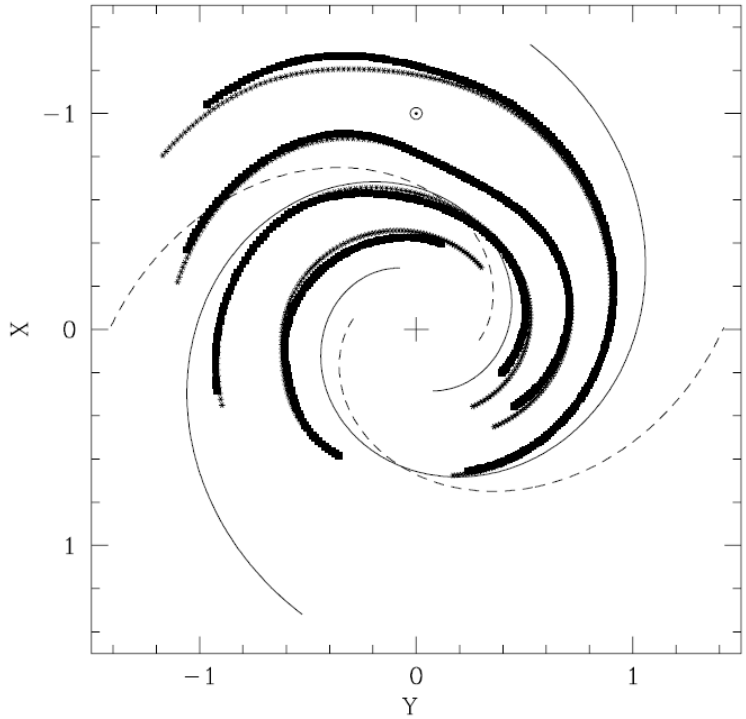

FIG. 19.—Schematic of the Galaxy showing the four spiral arms as mapped by H II regions and the dust (*bold lines*), the sheared arms in the *K* band (*stars*), and the arms in the two-arm logarithmic model for *J*- and *K*-band fit (*dashed*) and the *K*-band fit alone (*solid*) (Drimmel, & Spergel 2001). The H II spirals are incomplete on the opposite side of the Galaxy owing to lack of data.

Drimmel & Spergel 2001, ApJ 556, 181

Estructura espiral con distintos indicadores

TABLE 1

RECENT STUDIES OF SPIRAL ARMS IN THE MILKY WAY (1995–2001)[a]

Number of Spiral Arms	Figure and Reference	Observational Data Used
4	Fig. 2 in Johnston et al. (2001)	H I gas
4	Steiman-Cameron, Wolfire, & Hollenbach (2001)	[C II], [N II]
2	Fig. 4 in Fernandez et al. (2001)	Cepheids, OB stars
4	Fig. 4 in Fernandez et al. (2001)	Cepheids, OB stars
6	Fig. 6 in Lépine et al. (2001)	Cepheids, H II gas
4	Fig. 12 in Vallenari, Bertelli, & Schmidtobreick (2000)	V, I optical stars
4	Fig. 1 in Drimmel (2000)	Dust 240 μm
2	Fig. 2 in Drimmel (2000)	*K*-band old stars
4 outer	Fig. 16 in Fux (1999)	H I, CO gas
4	Table 1 in Mishurov & Zenina (1999)	Cepheids
2	Table 1 in Mishurov & Zenina (1999)	Cepheids
4	Fig. 15*b* in Englmaier & Gerhard (1999)	H I, CO, NIR COBE
4 outer	Fig. 14 in Sevenster (1999)	OH, IR stars
4	Fig. 4 in Han, Manchester, & Qiao (1999)	RM pulsars
4	Fig. 1 in Indrani & Deshpande (1999)	RM pulsars
4	Fig. 3 in Efremov (1998)	H I clouds
4	Fig. 4 in Amaral & Lépine (1997)	Nearby open clusters
…	Table 3 in Heiles (1996)	Polarized stars
4	Fig. 1 in Chen et al. (1996)	^{26}Al 1.8 MeV
4	Fig. 1 in Deshpande (1995)	Radio pulsars

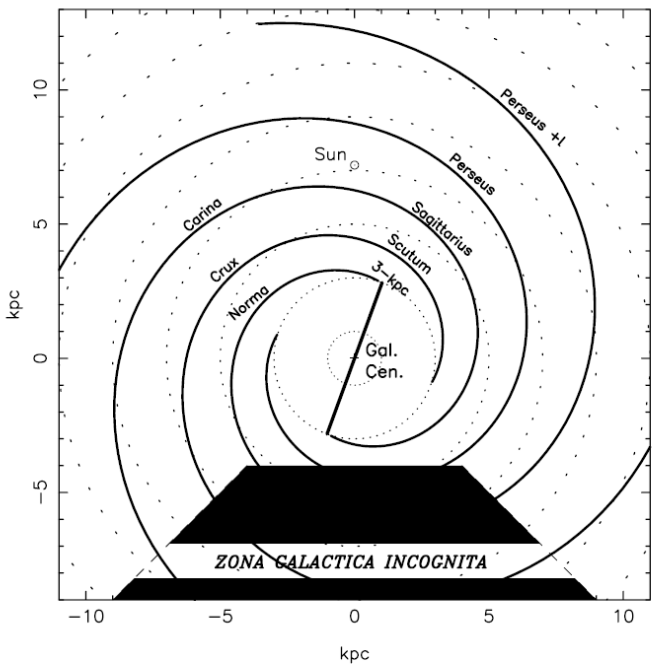

FIG. 2.—Model of logarithmic spiral arms, using the results of this metastudy ($p = 12°$ inward, $m = 4$). The logarithmic model was fitted to the Galactic longitude values of the tangents to the observed spiral arms as seen from the Sun. The Sun is shown by a circled dot, with the Sun–GC distance taken as 7.2 kpc (y-axis). A central bar extends radially from the GC to 3 kpc, inclined clockwise at an angle of 20° to the Sun–GC line. Dots show concentric circles around the GC, at a Galactic radius $r = 1, 3, 5, 7, 9, 11, 13$ kpc.

Vallée 2002, ApJ 566, 261

Estructura espiral con regiones HII y nubes molec. gig.

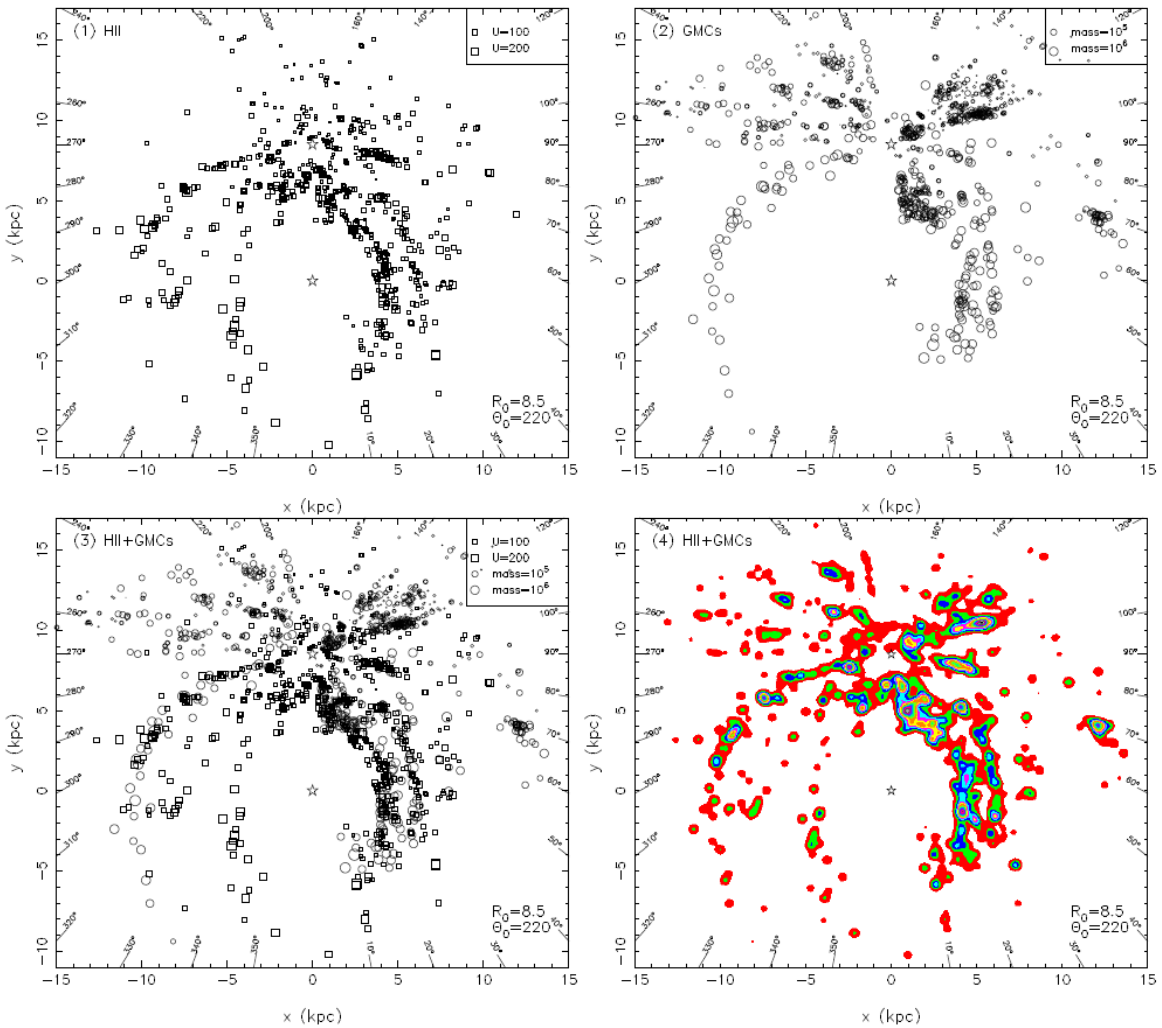

Fig. 3. *Panel (1)* is the distribution of HII regions, *Panel (2)* is the distribution of GMCs, and *Panel (3)* is the distribution of HII regions and GMCs together for illustration of the Galactic spiral structure. The solar parameters R_0=8.5 kpc and Θ_0=220 km s^{-1} were adopted. The coordinates originate from the Galactic center, and the Sun is located at (x = 0.0 kpc, y = 8.5 kpc). The open squares indicate the HII regions with the symbol area proportional to exciting parameters. The open circles indicate GMCs with the symbol size proportional to $log(M_{GMCs})$ (see Sect. 2.3). *Panel (4)* is the color distribution of both kinds of tracers, each brightened as a Gaussian with the amplitude of the weighting parameter, B, so that the spiral arms are clearly demonstrated.

Hou et al. 2009, A&A 499, 473

Estructura espiral y modelos

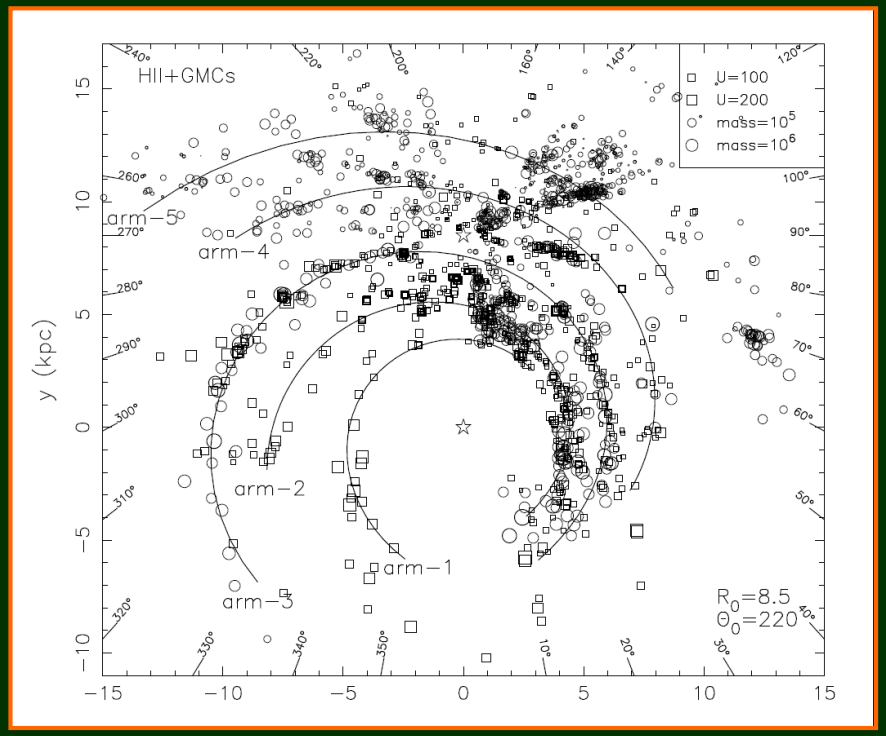

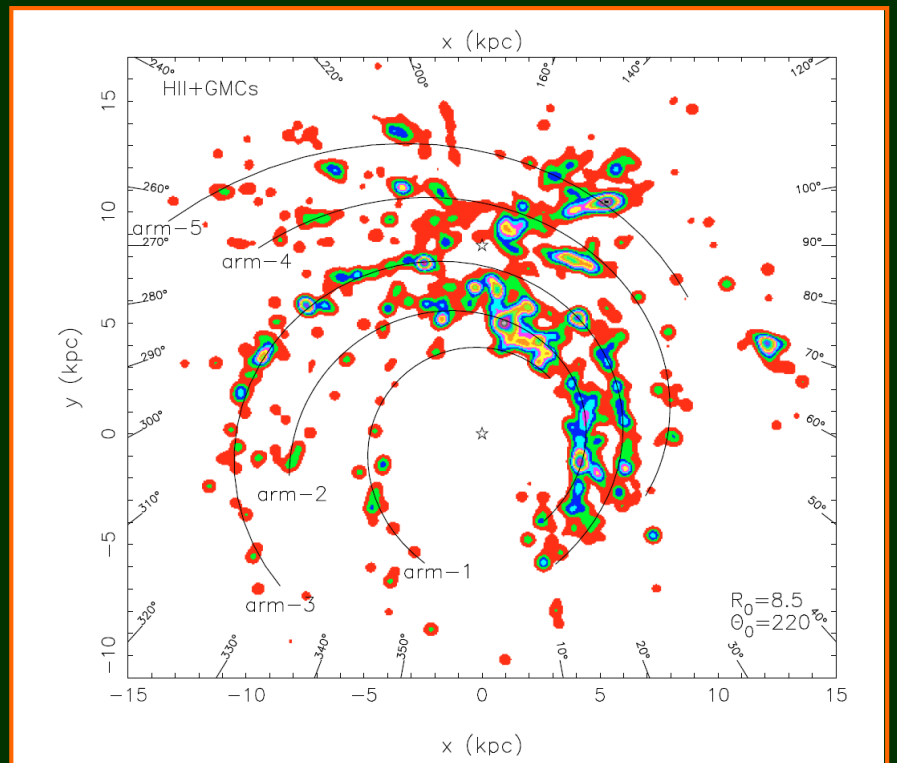

Fig. 7. The best-fitting polynomial logarithmic-arm model (R_0 = 8.5 kpc and Θ_0 = 220 km s^{-1}), plotted onto the data distribution (*top panel*) and the color brightened-tracer image (*bottom panel*) of tracers. Almost all main tracers are connected by the outlined arms, except for one complex at (x, y) = (12 kpc, 4 kpc) which either has an overestimated distance or it belongs to another outer arm.

Hou et al. 2009,
A&A 499, 473

Estructura del disco estelar externo con conteos del 2MASS

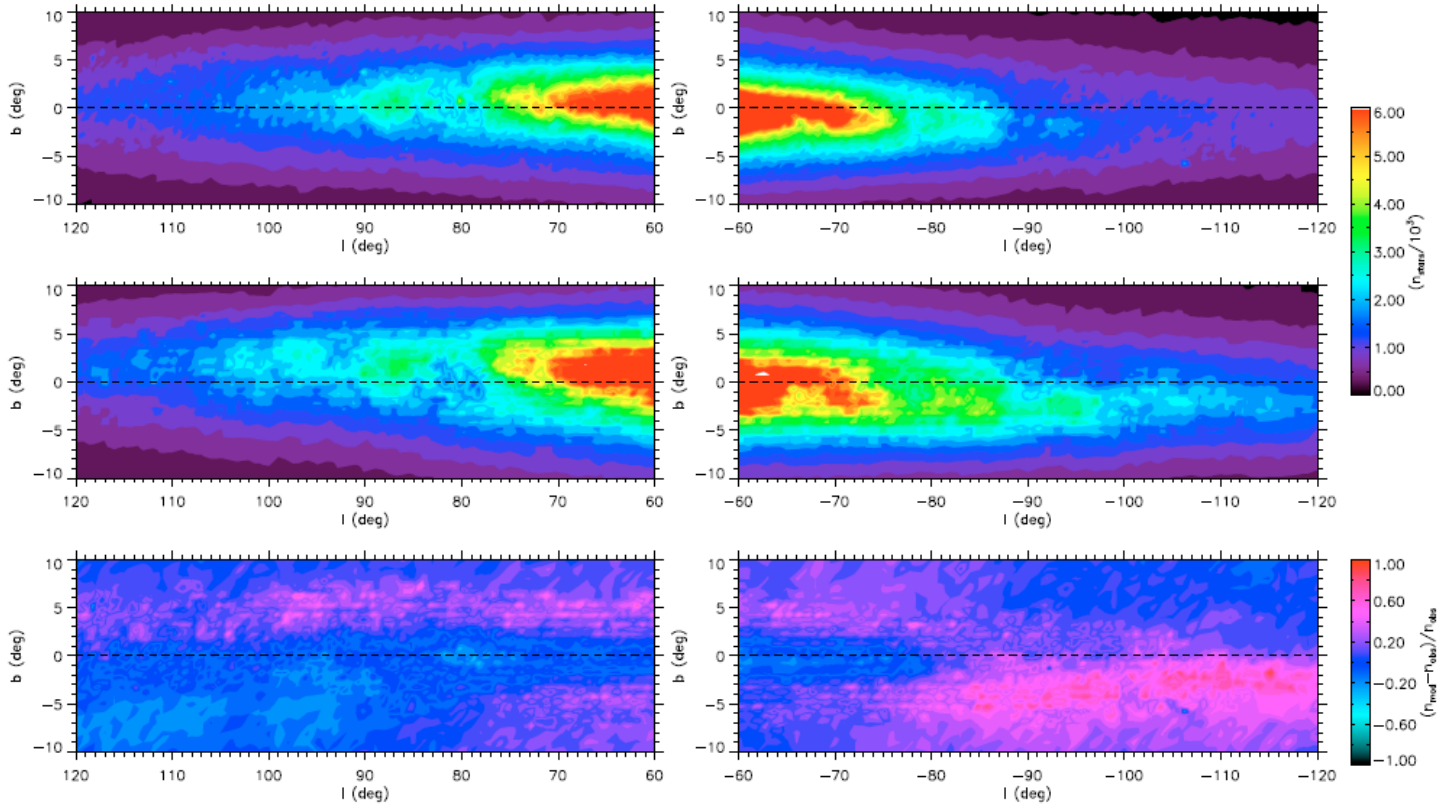

Fig. 3. 2MASS star counts (*top*), modelled ones (*middle*), and relative difference between the two (*bottom*) with $\gamma_{warp} = 0.18$ and $h_R = 2530$ pc. Dashed line indicates the $b = 0°$ plane. On the left is the northern warp, on the right the southern warp.

Reylé et al. 2009, A&A 495, 819

La Vía Láctea en 3D: observaciones de Cefeidas - proy. OGLE

"This 3D Map of the Milky Way Is the Best View Yet of Our Galaxy's Warped, Twisted Shape"

Map of the MilkyWay in three-dimensions based on the positions and distances of thousands of classical Cepheid variable stars.

Skowron et al. 2019, Science 365, 478

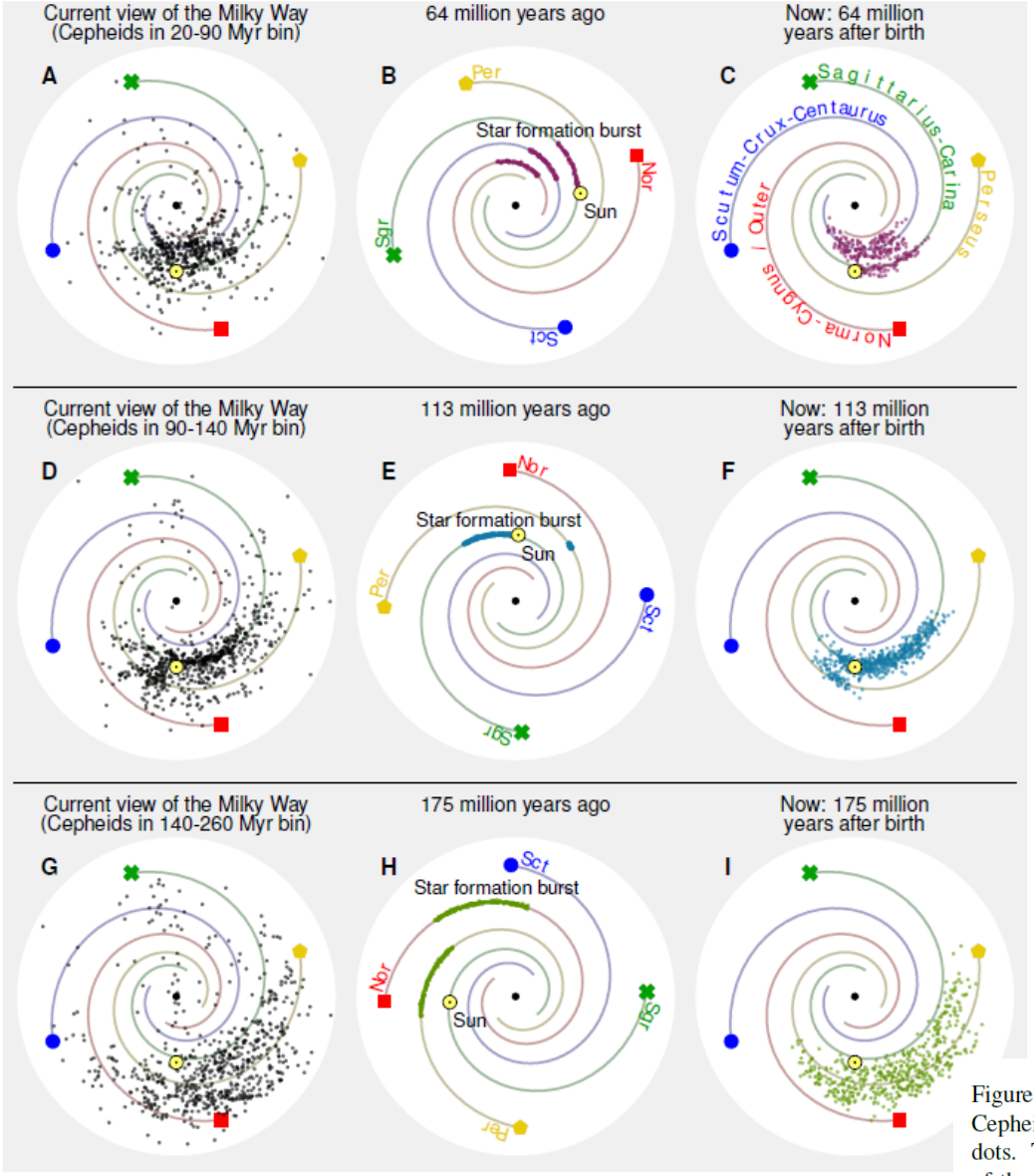

"Stars might have formed in bursts…"

Figure 4: **Possible origin of the Cepheid structures.** (**A**) Face-on view of our Galaxy, where Cepheids that belong to the age bin 20 to 90 Myr (median age 64 Myr) are shown with black dots. The Sun is marked with a yellow dot, the Galactic center with a black dot. Locations of the spiral arms: yellow pentagon, Perseus arm; green cross, Sagittarius-Carina arm; blue dot, Scutum-Crux-Centaurus arm; red square, Norma-Cygnus/Outer arm. (**B**) Location of the Galaxy's spiral arms 64 Myr ago, with simulated star formation regions along the Norma-Cygnus/Outer, Scutum-Crux-Centaurus and Sagittarius-Carina arms marked in violet. (**C**) Current location of stars from the simulated star formation region (violet). (**D** to **F**) Same as (A) to (C), but for the age bin 90 to 140 Myr with a median age of 113 Myr. (**G I**) Same as (A) to (C), but for the age bin 140 to 260 Myr with a median age of 175 Myr.

Skowron et al. 2019, Science 365, 478

La Vía Láctea en 3D: observaciones de Cefeidas - proy. OGLE

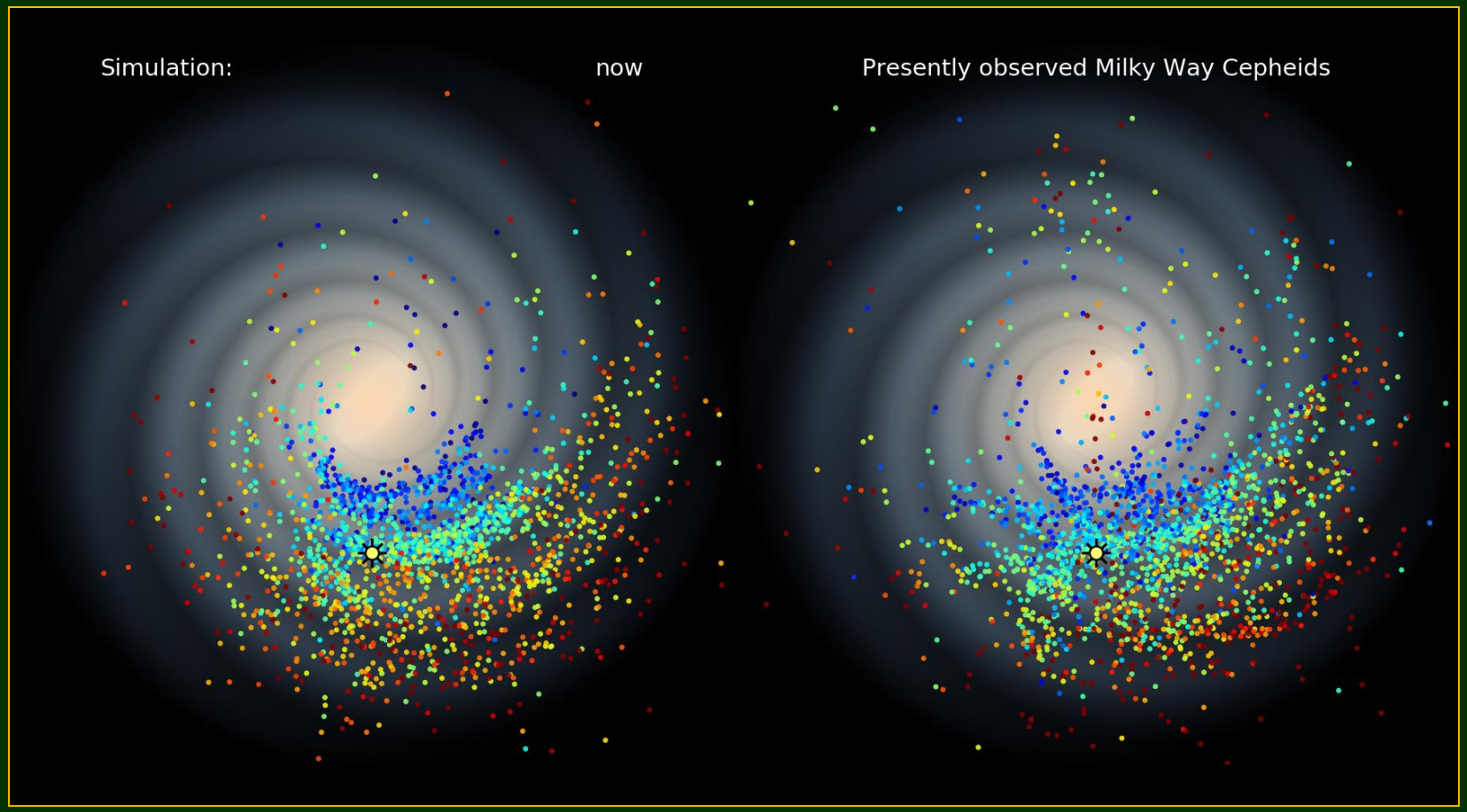

This image compares a simulation of the Milky Way galaxy's Cepheid star variables (left) with actual observations of their numbers (right). Red points indicate older stars, while younger ones are shown in blue.

Ejemplos de objetos típicos del *disco*

- Cúmulos abiertos o galácticos
- Nebulosas
  - de reflexión
  - de emisión
  - oscuras
- Polvo

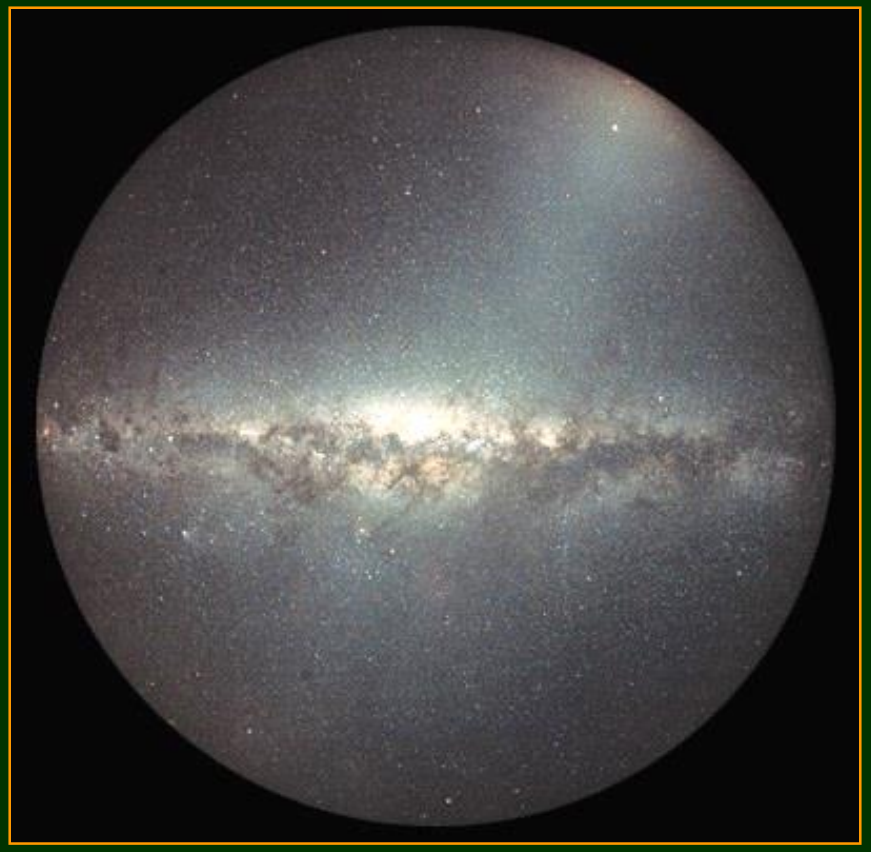

Cúmulo abierto: las Pleiades más de 3.000 estrellas

Credit & Copyright: Robert Gendler

Cúmulo abierto: M7 en Scorpius aprox. 100 estrellas

Credit & Copyright: Allan Cook & Adam Block, NOAO, AURA, NSF

Todos los tipos de nebulosas en el Complejo Molecular de Orión:

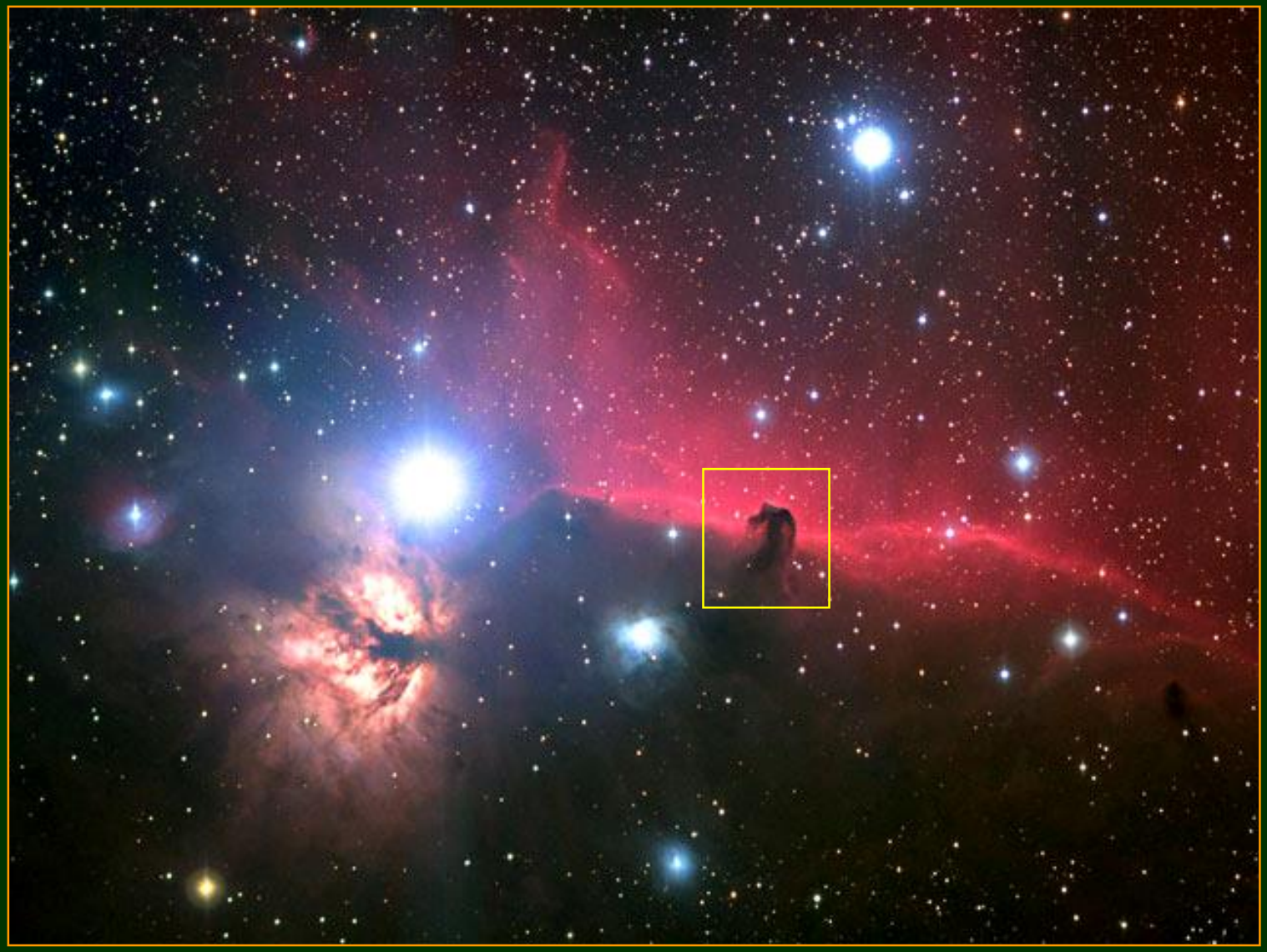

1.500 AL

Imagen compuesta con más de 20 hs de exposición

Image credit: Ron Brecher

Nebulosa oscura “Cabeza de Caballo”

Credit: Arne Henden (US Naval Observatory, Flagstaff)

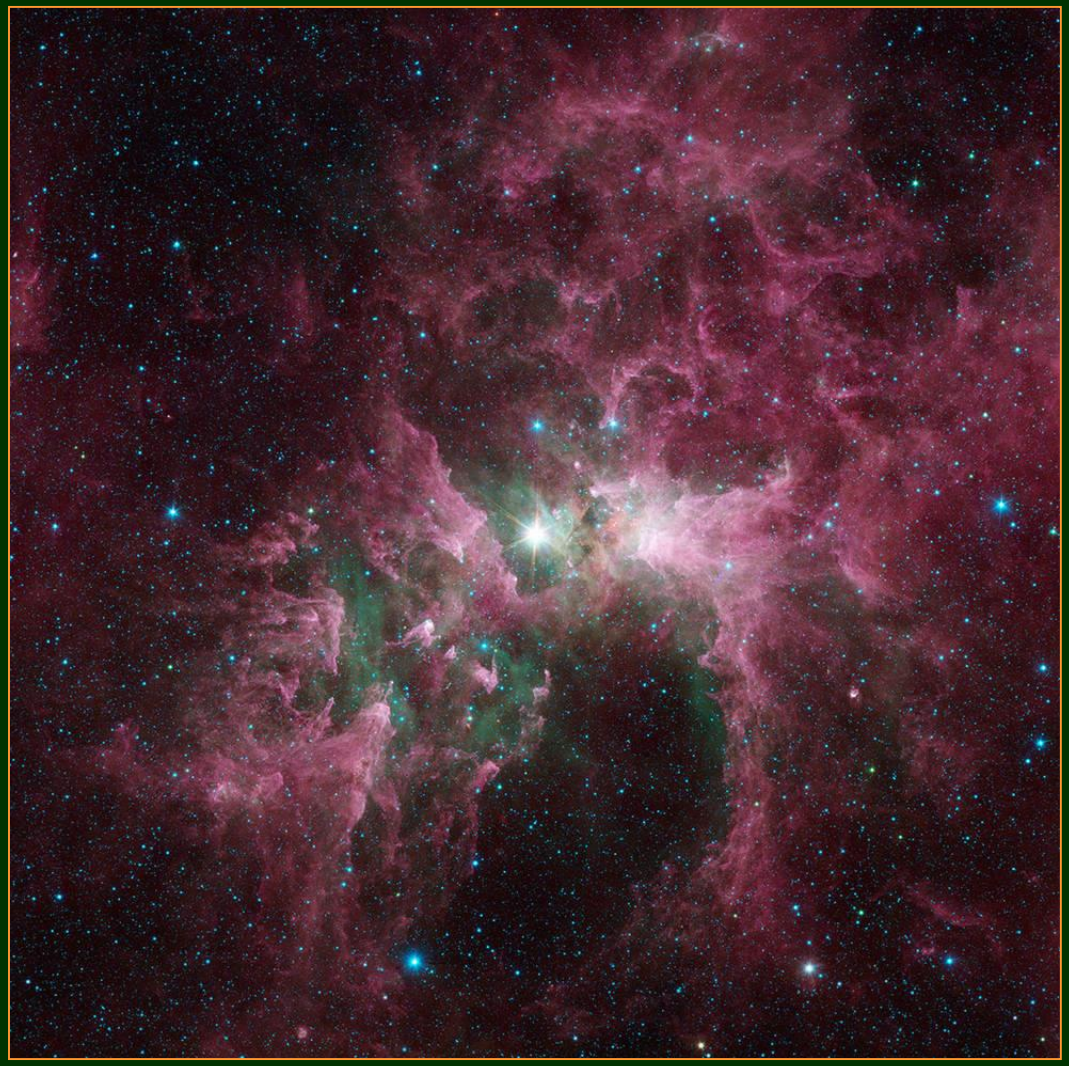

Nebulosa de Carina

Image credit: NASA/JPL-Caltech

The bright star at the center of this image is Eta Carinae, one of the most massive stars in the Milky Way galaxy. With around 100 times the mass of the Sun and at least 1 million times the brightness, Eta Carinae releases a tremendous outflow of energy that has eroded the surrounding nebula. Spitzer's infrared vision lets us see the dust, shown in red, as well as clouds of hot, glowing gas, which appear green.

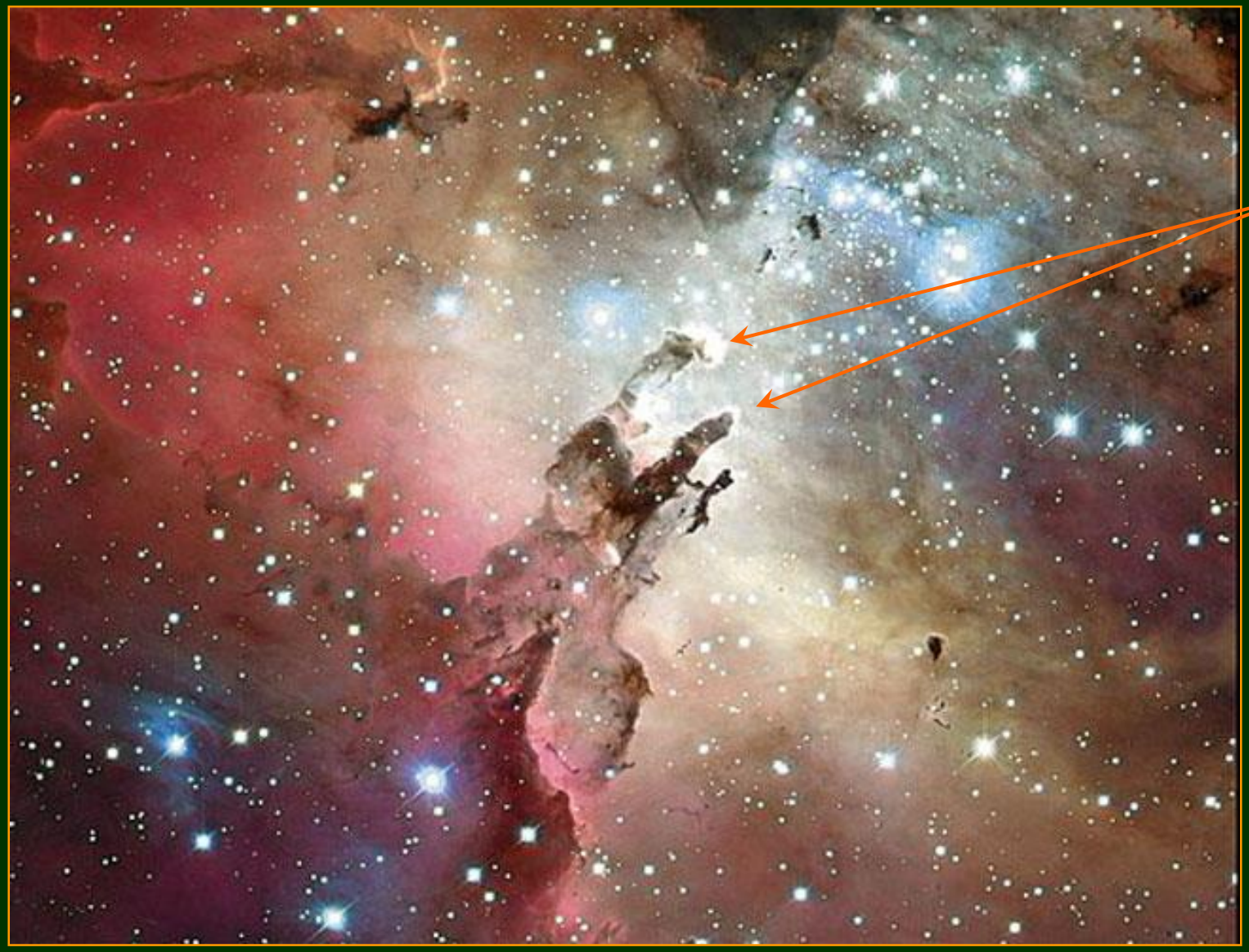

Detalle de la nebulosa del Águila y cúmulo abierto M16

Credit & Copyright: Jean-Charles Cuillandre (CFHT), Hawaiian Starlight, CFHT

N44F: nebulosa en forma de burbuja
en la Nube Mayor de Magallanes

formada por el viento de una estrella muy joven

imagen HST

Ejemplo de objetos típicos del *halo*

Cúmulo globular M3

aprox. 500.000 estrellas

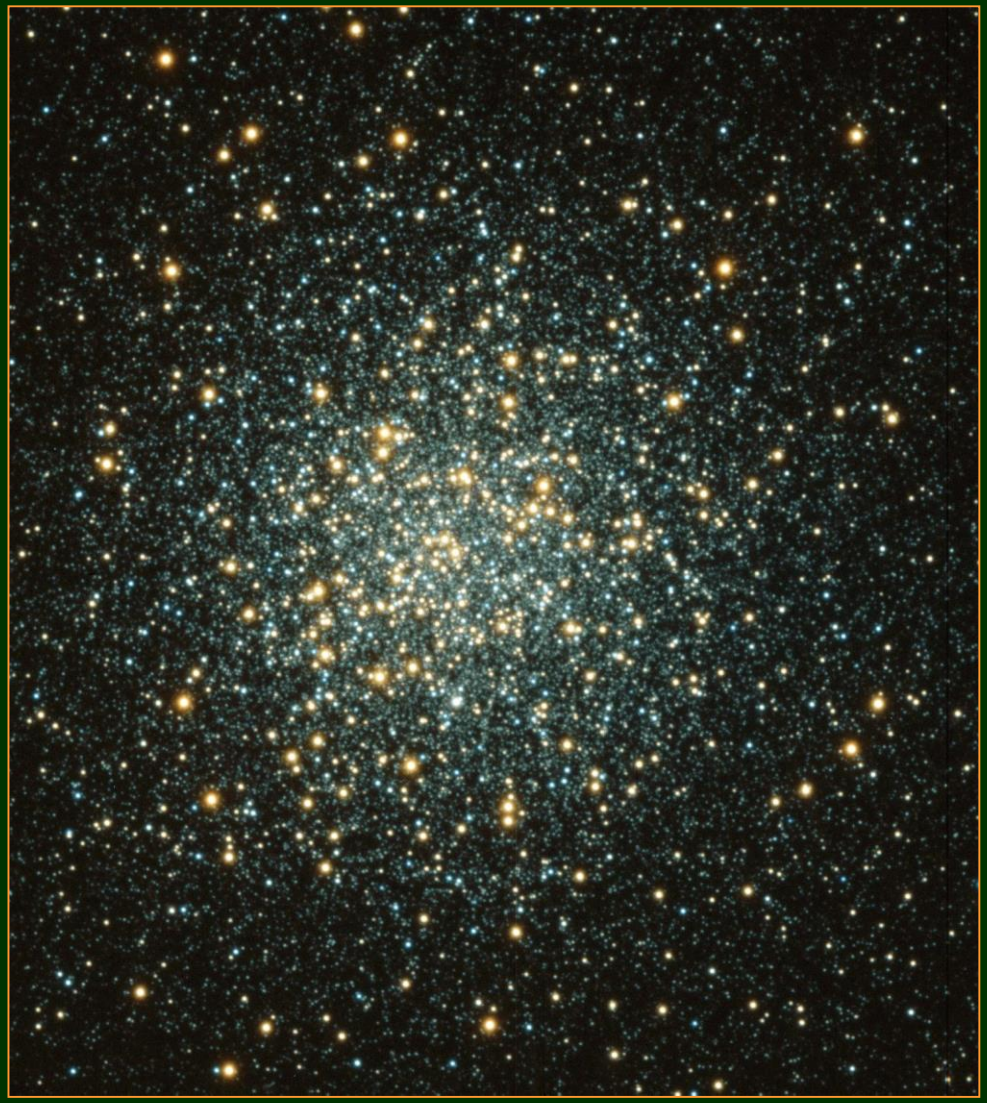

Credit & Copyright: S. Kafka & K. Honeycutt (Indiana University), WIYN, NOAO, NSF

Bulbo: observ. del relevamiento ARGOS

We present the metallicity results from the ARGOS spectroscopic survey of the Galactic bulge. Our aim is to understand the formation of the Galactic bulge: did it form via mergers, as expected from ΛCDM theory, or from disk instabilities, as suggested by its boxy/peanut shape, or both?

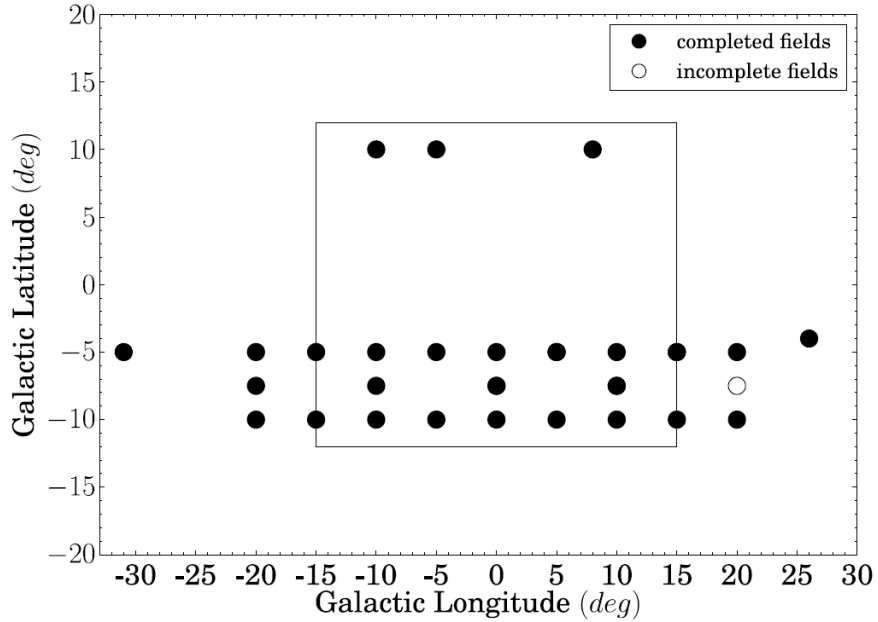

Figure 1. The 28 x 2° fields in our survey, in Galactic latitude and longitude. Filled circles indicate fields for which we have complete data. One field at $(l, b) = (20°, -7.5°)$ is incomplete; only 600 stars were observed for this field. The rectangle denotes the approximate extent of the boxy/peanut-bulge

espectros de 28000 estrellas en 28 campos

Ness et al. 2013,
(a) MNRAS, 430, 836
(b) MNRAS, 432, 2092

Bulbo: distribución de metalicidades

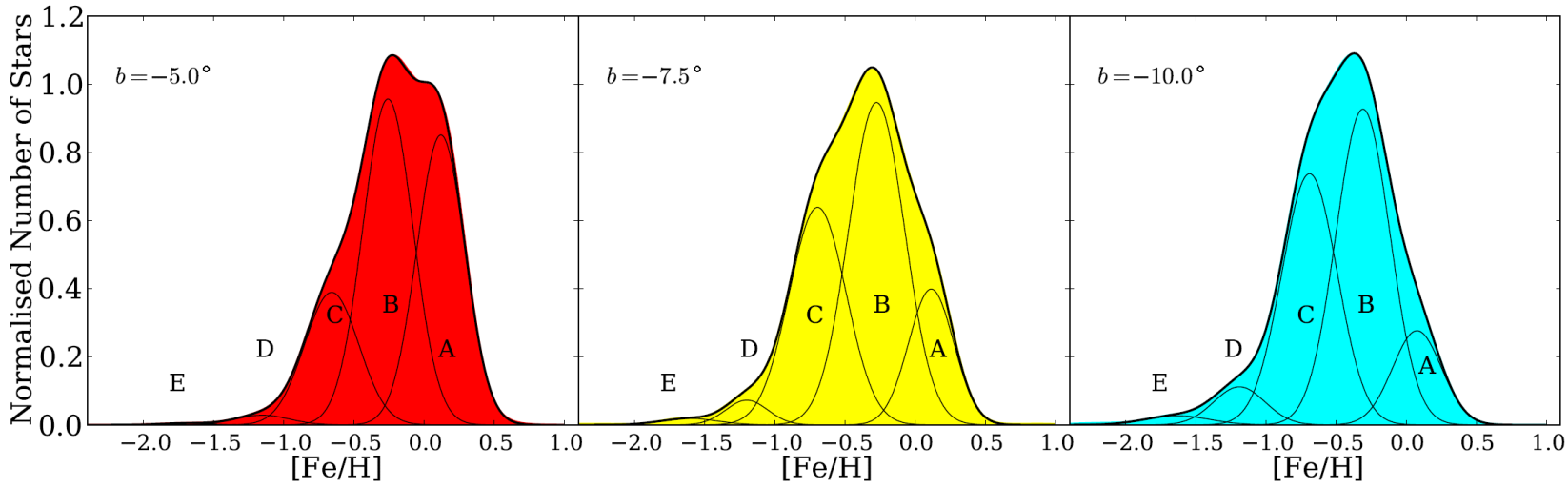

Figure 1. MDFs for stars within $R_G < 3.5$ kpc at from left to right $b = -5°$, $b = -7.5°$ and $b = -10°$, for $l = \pm 15°$, showing the changing contribution of metallicity fractions with latitude.

Ness et al. 2013b

Bulbo: modelo galáctico

"As the disk becomes unstable, it forms a rotating bar which buckles and heats the disk vertically. The orbits of the stars originally in the bar are extended vertically into orbits which now define the boxy/triaxial / peanut-shaped bulge."

Ness et al. 2014, ApJ 787, L19

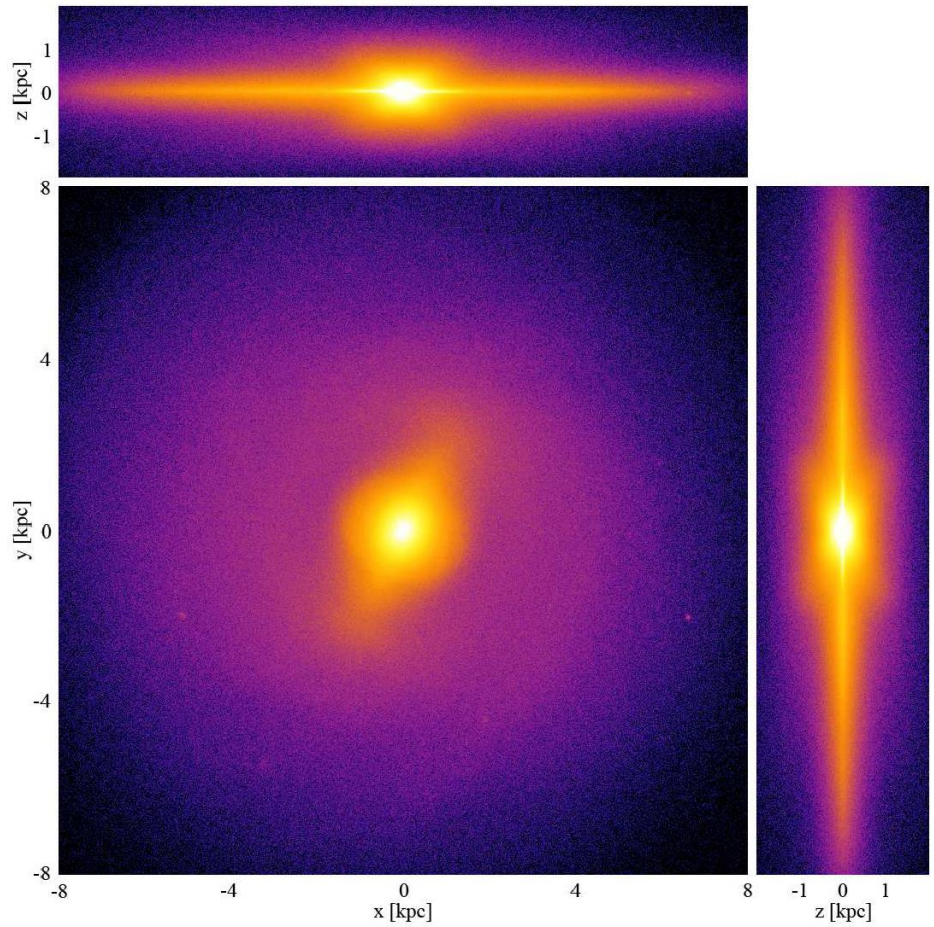

Fig. 2.— Mass surface density of the model projected onto the $x-y$, $x-z$ and $y-z$ planes as indicated. Note the boxy shape and X-structure in the $y-z$ projection at right.

Using an N-body+SPH simulation of a disk galaxy forming out of gas cooling inside a dark matter halo and forming stars, we find a qualitative agreement between our model and the observations of young metal-rich stars in the bulge.

“The X-shaped Bulge of the Milky Way Revealed by WISE”

Ness et al. 2016, AJ,152, 14

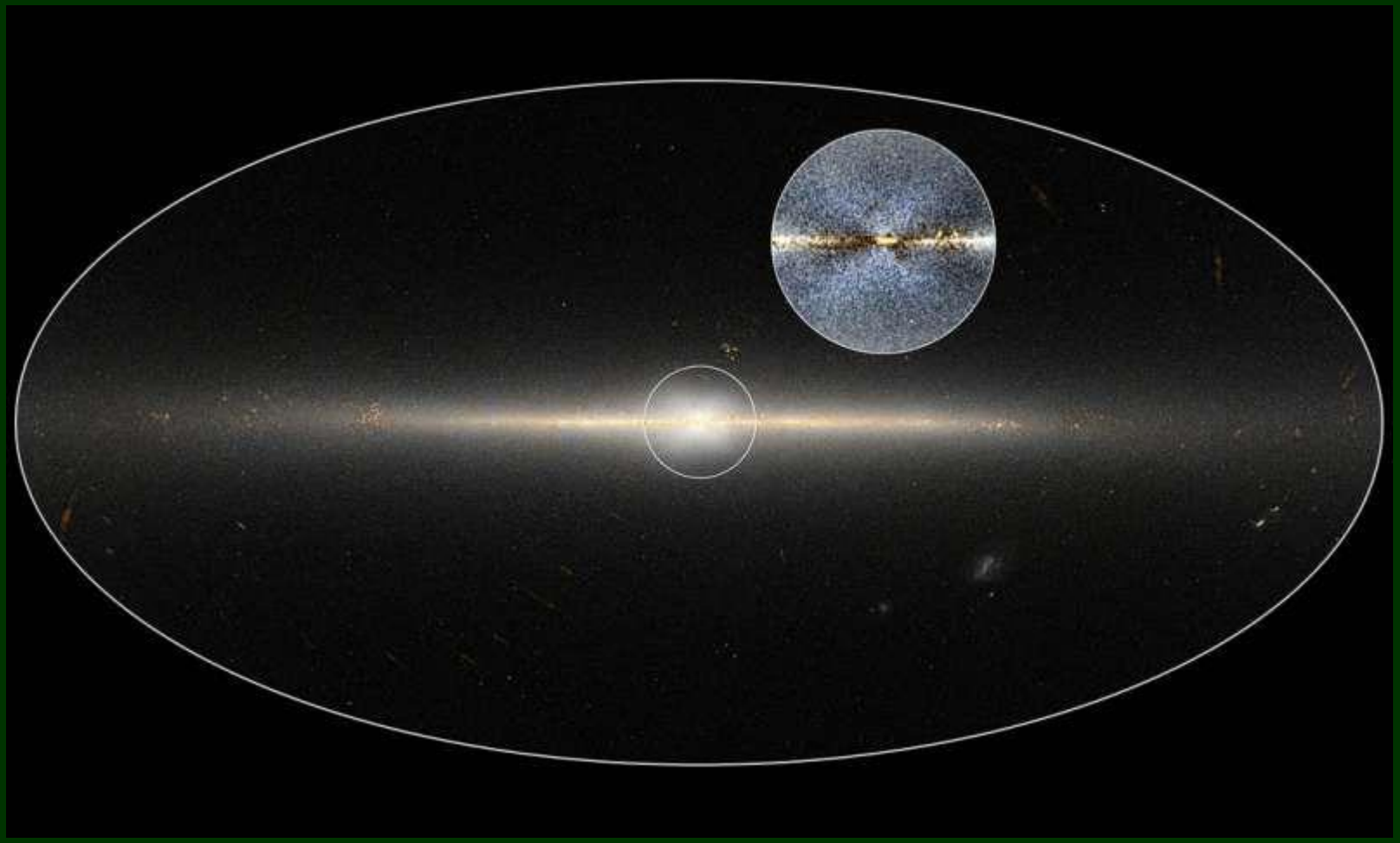

Wide-Field Infrared Survey Explorer (WISE; Wright et al. 2010) is a full sky photometric survey, using four bands in the ~mid-infrared at **3.4, 4.6, 12 and 22 μ.**

Bulbo: conteos en NIR

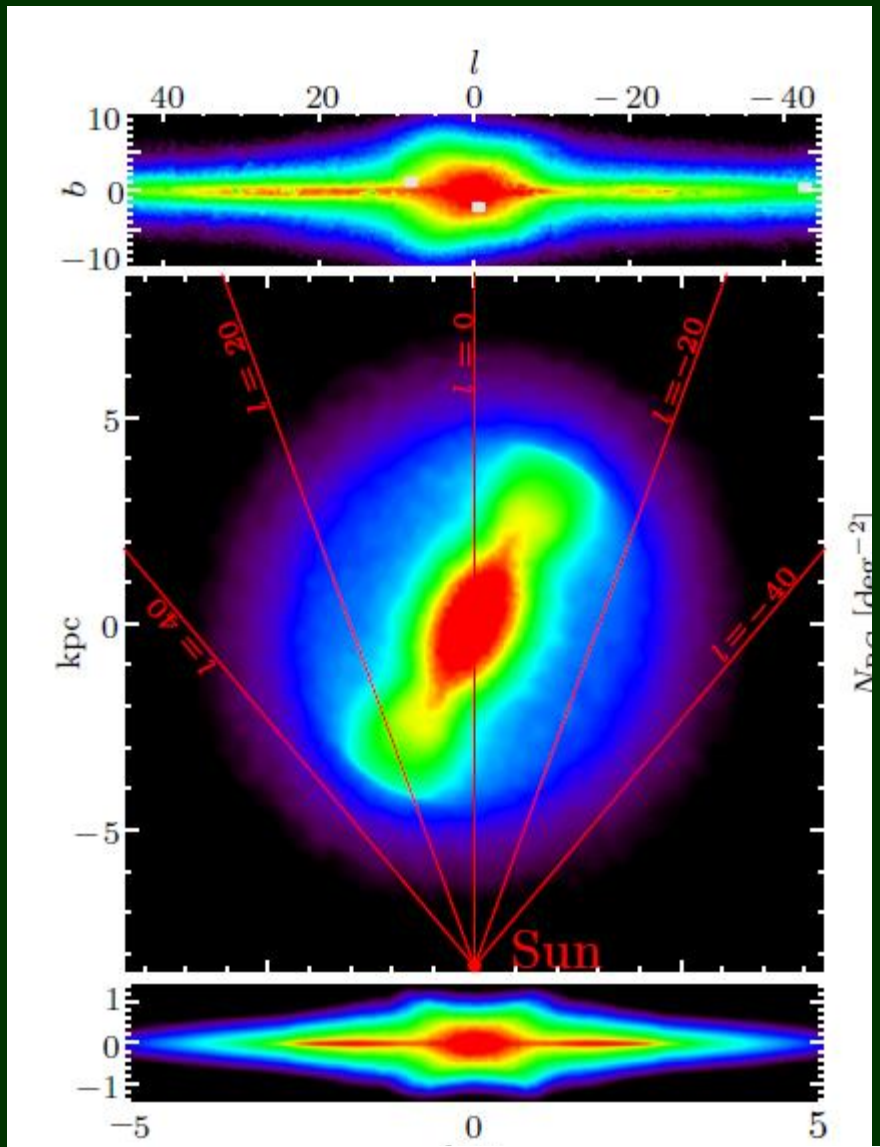

Wegg et al. 2015, MNRAS, 450, 4050

Left: projections of the Galactic b/p-bulge and long bar reconstructed from NIR star counts. Top: inner Galaxy as seen from the Sun, in bright star counts complete across several NIR surveys. Middle: Projection of best-fitting RCG star count model as seen from the North Galactic Pole. Viewing directions from the Sun are indicated for longitudes $|l| = 0°, 20°, 40°$. Bottom left: side-on view showing the transition from the b/p bulge to the long bar and disk. Right: Vertical

Barra: posición y orientación en el plano

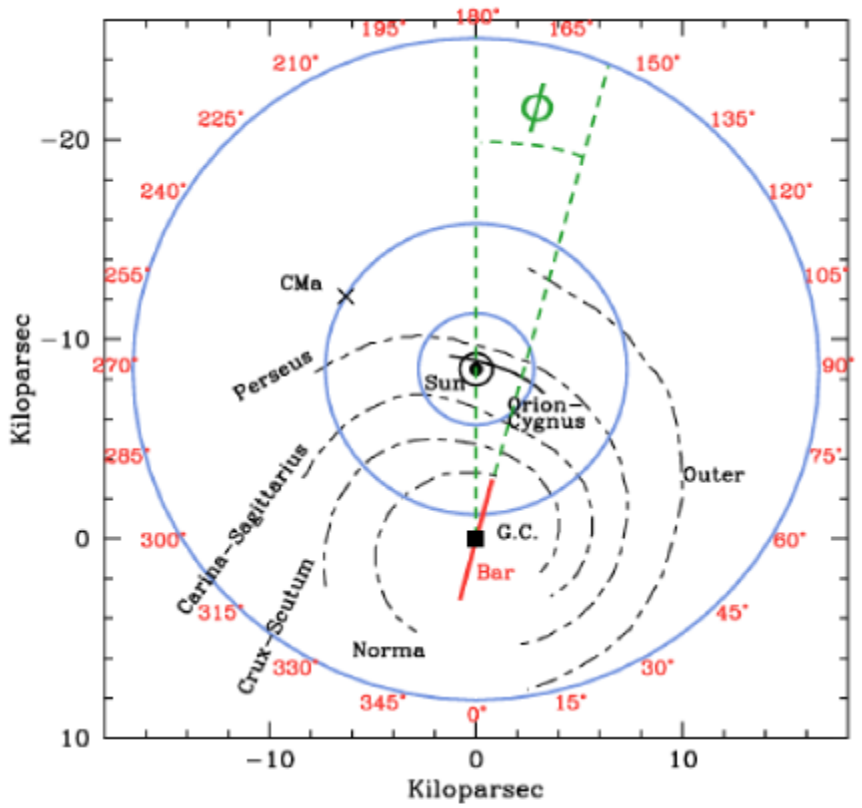

Figure 11

Plan elevation of the Galactic disk centred on the Sun's position showing the orientation and location of the main spiral arms. The numbered outer circle defines galactic longitude (ℓ). The Canis Major (CMa) overdensity is in the same general direction as the maximum disk warp (Courtesy of Momany et al. 2006).

Barra:
long. total: 10 kpc
ϕ = 28 - 33°
masa: 10^{10} M⊙
Vrot ~ 100 km/s

Bland-Hawthorn & Gerhard 2016, ARAA 54, 529

Esquema: Sagittarius dwarf tidal stream

(desintegración de la galaxia enana de Sagitario)

Drawing Credit & Copyright: David Martinez-Delgado (MPIA) & Gabriel Perez (IAC)

The Sagittarius Dwarf Tidal Stream(s)

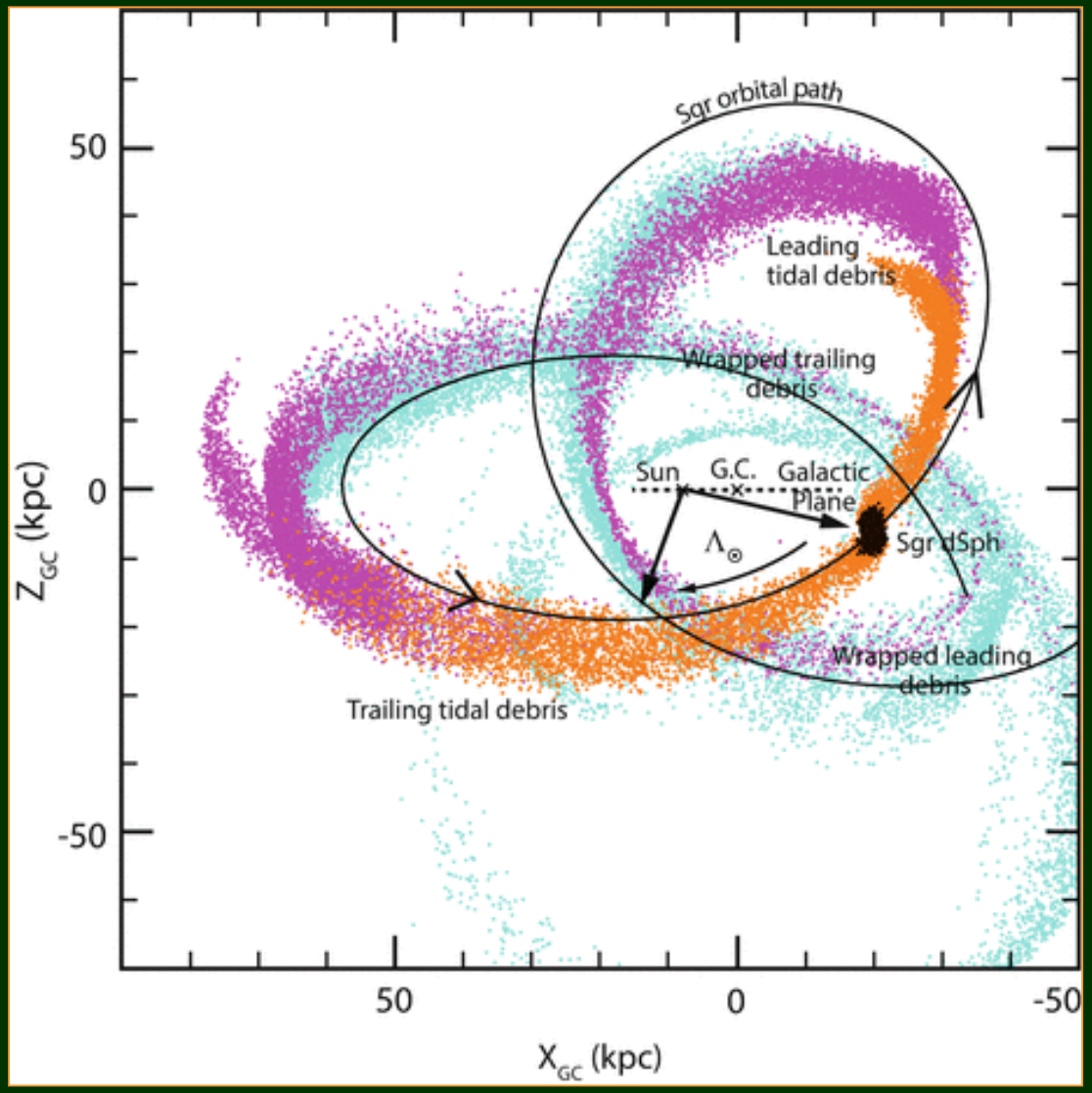

Law & Majewski, 2016, ASSL, 420, 31

STREAMS IN THE HALO

Modelo teórico de la estructura del halo:

"cosmologically self-consistent model for the formation of the stellar halo in Milky Way–type galaxies, focused specifically on the role of stellar accretion events in the halo formation process."

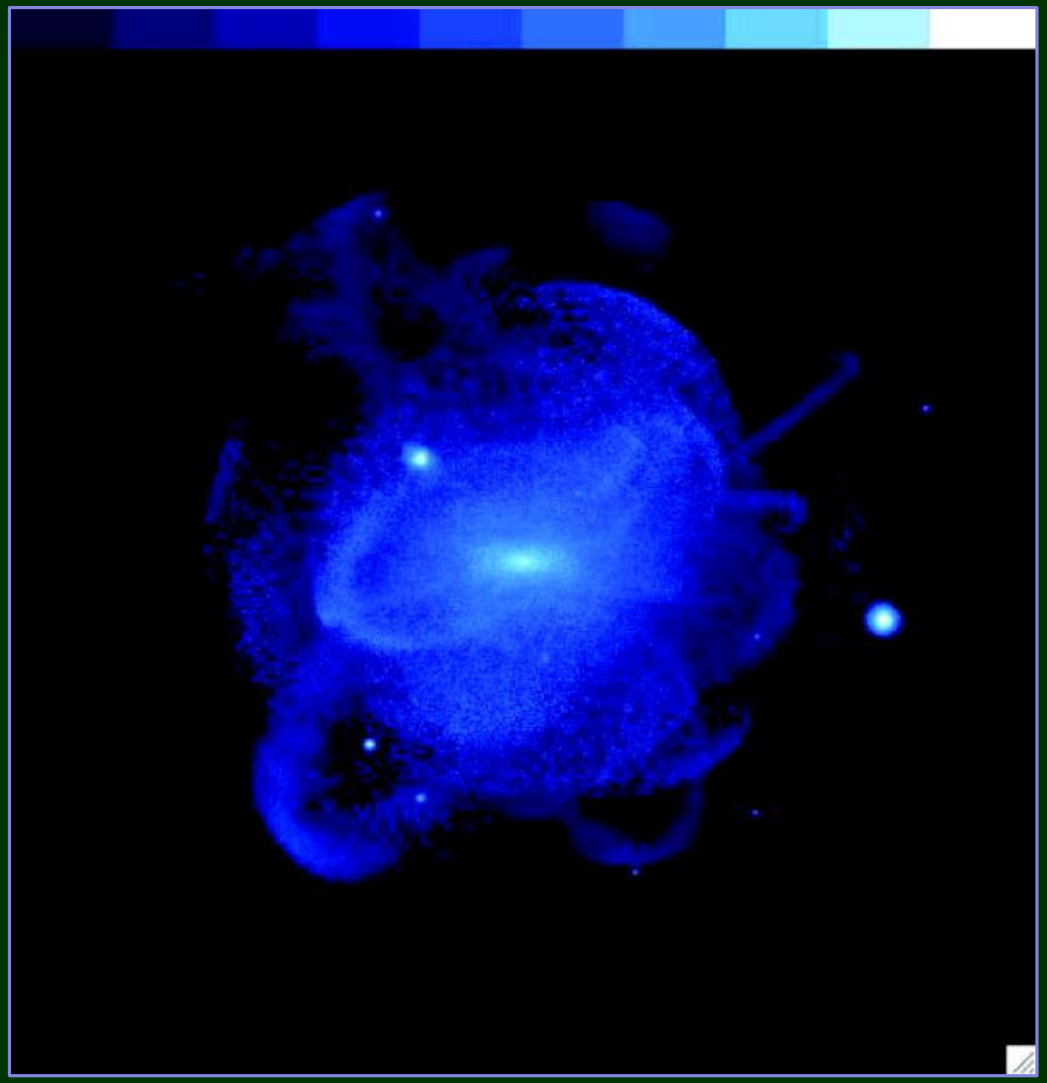

Bullock & Johnston 2005, ApJ, 635, 931

Map of stars in the outer regions of the Milky Way Galaxy, derived from the SDSS (northern sky)

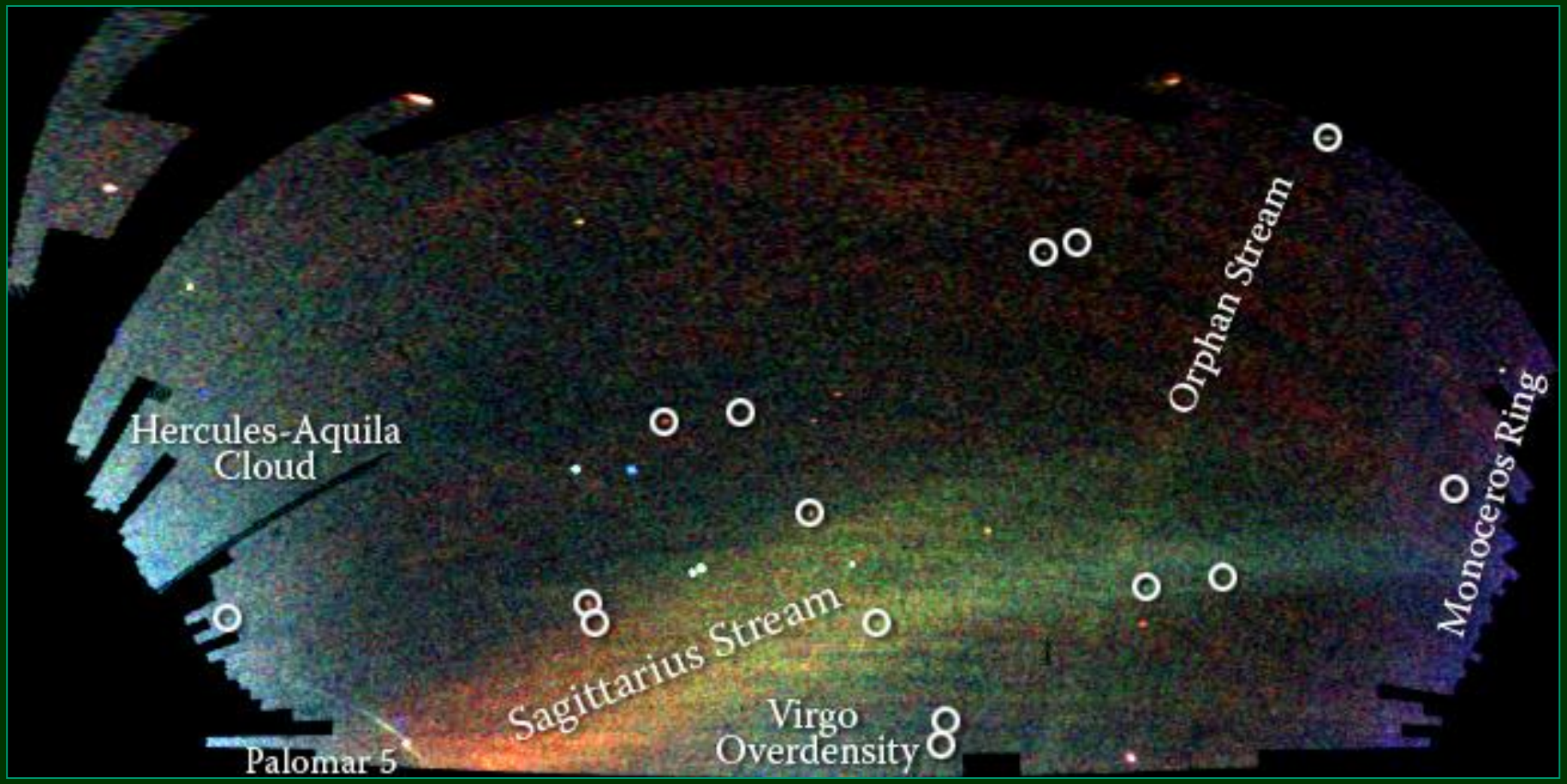

color indicates the distance of the stars,
while the intensity indicates the density of stars on the sky

Credit: V. Belokurov and the Sloan Digital Sky Survey

Milky Way stellar streams

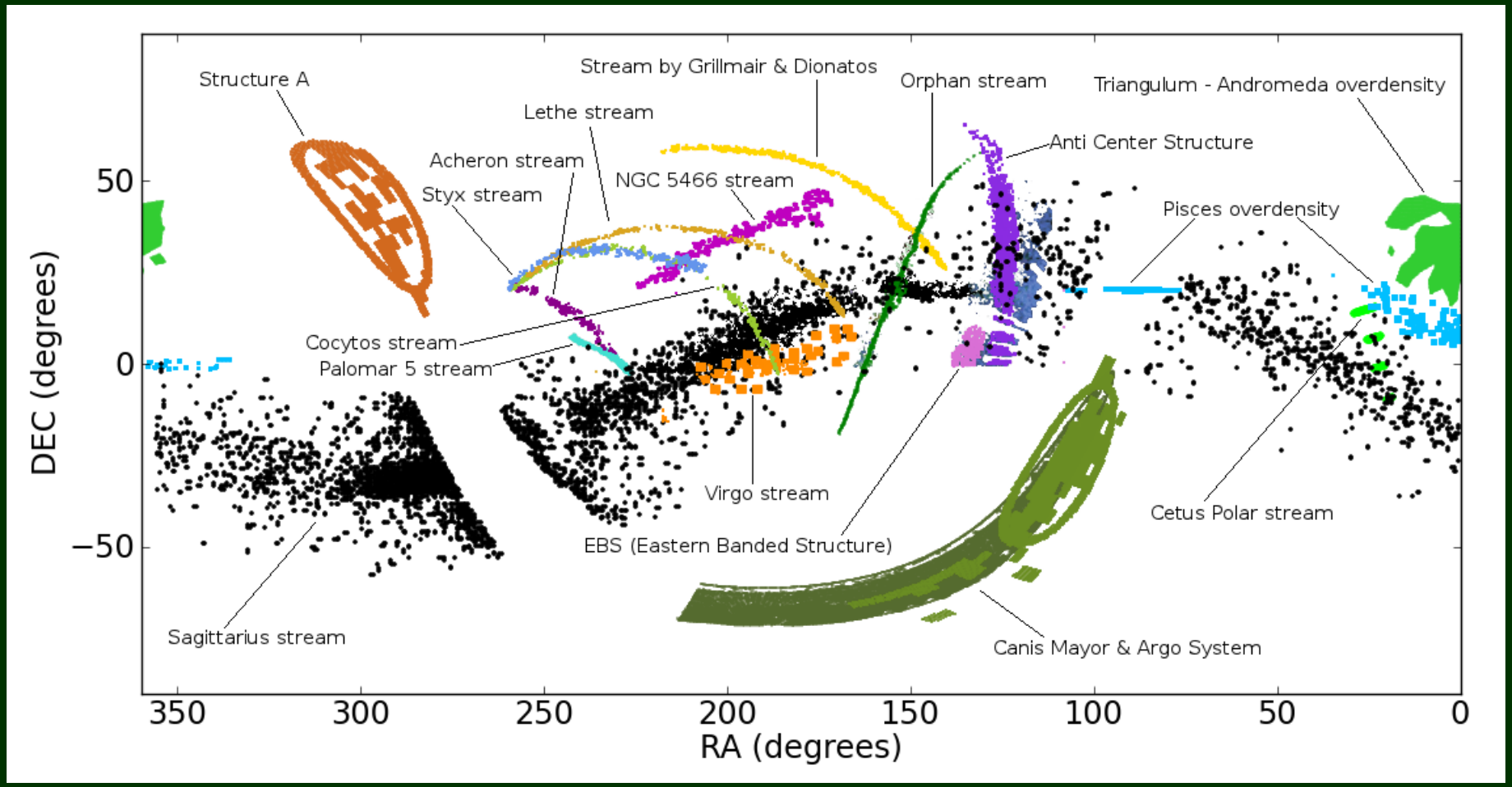

Milky Way distribution of spatially coherent streams - labelled
Equatorial projected distribution of Milky Way spatially coherent streams.

Credit: B. Pila Díez, Local Group inventory of dwarf galaxies and stellar streams (Leiden Univ.)

Formación del "*disco grueso*" :

Gaia-Sausage (Gaia-Enceladus) merger

Belokurov et al. (2020, MNRAS):

- Dwarf stellar mass (prior to disruption) = 5 x 10^9 M⊙

-Merger: ~10 Gyr ago

Helmi et al. (2018, Nature 563, 85):

- "the inner halo is dominated by debris from an object that at infall was slightly more massive than the Small Magellanic Cloud, and which we refer to as Gaia–Enceladus. The stars that originate in Gaia–Enceladus cover nearly the full sky, and their motions reveal the presence of streams and slightly retrograde and elongated trajectories."

- "led to the dynamical heating of the precursor of the Galactic thick disk"